OUTER RISE SEISMICITY OF THE SUBDUCTING NAZCA PLATE: PLATE STRESS DISTRIBUTION, FAULT ORIENTATION AND PLATE HYDRATION

Louisa Barama, B.S.

An Abstract Presented to the Graduate Faculty of
Saint Louis University in Partial Fulfillment
of the Requirements for the Degree of
Master of Science

2014

ABSTRACT

Subduction of the Nazca plate beneath the South American plate drives frequent and sometimes large magnitude earthquakes. During the past 40 years, significant numbers of outer rise earthquakes have occurred in the offshore regions of Colombia and Chile. In this study, we investigate the distribution of stress due to lithospheric bending and the extent of faults within the subducting plate. To calculate more accurate epicenters and to constrain which earthquakes occurred within the outer rise, we use hypocentroidal decomposition to relocate earthquakes with Global Centroid Moment Tensor (GCMT) solutions occurring after 1976 offshore Colombia and Chile. We determine centroid depths of outer rise earthquakes by inverting teleseismic P-, SH-, and SV- waveforms for earthquakes occurring from 1993 to 2014 with $M_w \geq 5.5$. In order to further constrain the results of the waveform inversion, we estimate depths by comparing earthquake duration, amplitude, and arrival times for select stations with waveforms with good signal to noise ratios. Our results indicate that tensional earthquakes occur at depths down to 13 km and 24 km depth beneath the surface in the Colombia and Chile regions, respectively. Since faulting within the outer rise can make the plate susceptible to hydration and mantle serpentinization, we therefore infer the extent of possible hydration of the Nazca plate to extend no deeper than the extent of tensional outer rise earthquakes.

OUTER RISE SEISMICITY OF THE SUBDUCTING NAZCA PLATE: PLATE STRESS DISTRIBUTION, FAULT ORIENTATION AND PLATE HYDRATION

Louisa Barama, B.S.

A Thesis Presented to the Graduate Faculty of
Saint Louis University in Partial Fulfillment
of the Requirements for the Degree of
Master of Science
2014

COMMITTEE IN CHARGE OF CANDIDACY:

Assistant Professor Linda Warren;
Chairperson and Advisor

Professor Robert Herrmann

Professor Lupei Zhu

ACKNOWLEDGEMENTS

I would like express my gratitude to my advisor Dr. Linda Warren and committee member Dr. Robert Herrmann for their guidance, knowledge and critical scientific insight. A special thank you to Erica Emry for her help, guidance, and for sharing her knowledge and research of the outer rise. Without them this research would not have been possible, and I consider it an honor to have worked with them. And lastly, thank you to my family, friends, and all who have supported me throughout this process

TABLE OF CONTENTS

List of Tables.....iv

List of Figures.....v

CHAPTER 1: INTRODUCTION.....1

CHAPTER 2: LITURATURE REVIEW
The Outer Rise.....3
Subduction Zone Water Cycle and Outer Rise Earthquakes.....4
Structure of the Nazca Plate Offshore South America and Previous Studies.....7
Previous Studies of the Nazca Plate Outer Rise.....10

CHAPTER 3: EARTHQUAKE RELOCATION
Data and Methods.....12
Results - Colombia.....13
Results - Chile.....14

CHAPTER 4: WAVEFORM INVERSION AND DEPTH DETERMINATION
Earthquake Selection and Data.....18
Method.....20
Results.....23

CHAPTER 5: DISCUSSION.....31

CHAPTER 6: CONCLUSIONS
Conclusion and Future Work.....38

Appendix.....39
Bibliography.....66
Vita Auctoris.....71

LIST OF TABLES

Table 3.1: Colombia GCMT and relocated latitudes and longitudes.....13

Table 3.2: Chile GCMT and relocated latitudes and longitudes..…...……..….....15

Table 4.1: Source-Side 4.0 km water layer Velocity Model..…...……..….....21

Table 4.2: Receiver -Side Continental Model.....…...……..….....22

Table 4.3: Waveform Inversion and Focal Depth Calculation Results..……..….....29

LIST OF FIGURES

Figure 2.1: Lithospheric Flexure Model...3

Figure 2.2: Plot of South America GCMT Earthquakes...9

Figure 3.1: Colombia Relocated Epicenters...14

Figure 3.2: Chile Relocated Epicenters ...17

Figure 4.1: Earthquakes Used for Waveform Inversion...19

Figure 4.2: Waveform Model Comparison...24

Figure 4.3: Inversion Plots for the 10/21/2010 Earthquake...27

Figure 4.4: Depth Estimation Plots for the 10/21/2010 Earthquake ...28

Figure 5.1: Depth vs. Latitude Plot...32

Figure 5.2: Colombia Offshore Geology and Study Events...36

Figure A.1.1 Waveform Inversion Results for the 11/26/1994 Earthquake...40

Figure A.1.2 Depth Estimation Plot for 11/26/1994 Earthquake...41

Figure A.2.1 Waveform Inversion Results for the 02/19/1996 Earthquake ...42

Figure A.2.2 Depth Estimation Plot for 02/19/1996 Earthquake...43

Figure A.3.1 Waveform Inversion Results for the 04/01/1998 Earthquake...44

Figure A.3.2 Depth Estimation Plot for 04/01/1998 Earthquake...45

Figure A.4.1 Waveform Inversion Results for the 12/20/2000 Earthquake...46

Figure A.4.2 Depth Estimation Plot for 12/20/2000 Earthquake...47

Figure A.5.1 Waveform Inversion Results for the 03/03/2001 Earthquake...48

Figure A.5.2 Depth Estimation Plot for 03/03/2001 Earthquake...49

Figure A.6.1 Waveform Inversion Results for the 04/09/2001 Earthquake...50

Figure A.6.2 Depth Estimation Plot for 04/09/2001 Earthquake...51

Figure A.7.1 Waveform Inversion Results for the 12/21/2002 Earthquake.....52

Figure A.7.2 Depth Estimation Plot for 12/21/2002 Earthquake.....53

Figure A.8.1 Waveform Inversion Results for the 11/12/2003Earthquake.....54

Figure A.8.2 Depth Estimation Plot for 11/12/2003 Earthquake.....55

Figure A.9.1 Waveform Inversion Results for the 07/16/2006 Earthquake.....56

Figure A.9.2 Depth Estimation Plot for 07/16/2006 Earthquake.....57

Figure A.10.1 Waveform Inversion Results for the 03/17/2007 Earthquake.....58

Figure A.10.2 Depth Estimation Plot for 03/17/2007 Earthquake.....59

Figure A.11.1 Waveform Inversion Results for the 03/18/2007 Earthquake.....60

Figure A.11.2 Depth Estimation Plot for 03/18/2007 Earthquake.....61

Figure A.12.1 Waveform Inversion Results for the 11/22/2009 Earthquake.....62

Figure A.12.2 Depth Estimation Plot for 11/22/2009 Earthquake.....63

Figure A.13.1 Waveform Inversion Results for the 06/28/2010 Earthquake.....64

Figure A.13.2 Depth Estimation Plot for 06/28/2010 Earthquake.....65

CHAPTER 1: INTRODUCTION

The majority of the Earth's seismicity occurs in subduction zones. The largest and most common of these earthquakes are thrust and megathrust earthquakes along the plate interface. However, there is abundant seismicity in the upward bulge in a subducting plate, called the outer rise, seaward of the trench. The outer rise is created due to elastic plate flexure as the down-going plate bends at the trench in subduction zones [*Caldwell et al.,* 1976; *Chapple et al.,* 1979]. Stress builds up in the outer rise primarily due to the bending of the uppermost lithosphere and is released in the form of faulting and brittle failure, referred to as tensional outer rise earthquakes. Outer rise events are not solely caused by the brittle faulting due to lithospheric bending. Other forces, such as the gravitational pull of the sinking plate and coupling with the overriding plate, can affect seismicity in the outer rise [*Kanamori*, 1971; *Christensen and Ruff,* 1988]. We can use earthquakes to study stress distribution throughout the subducting plate by determining where earthquakes occur, at what depths, and in which direction the faults rupture and slip. Studies of outer rise seismicity can provide constraints on mantle composition, local deformation, plate interface slip and coupling, and plate hydration [*Chapple and Forsyth*, 1979; *Lay et al.,* 1989; *Rüpke et al.,* 2004; *Hirschmann,* 2006].

Knowledge and understanding of the amount of water in the subducting plate is critical for understanding the strength or weakness of the plate interface. Extensive hydration of a subducting plate prior to subduction can affect the Earth's water cycle [*Lefeldt and Grevemeyer*, 2008], subduction arc and back-arc volcanism and, if the faults penetrate deep enough, can react with the lithospheric mantle [*Lefeldt et al.,* 2009]. In addition, hydration at the surface and subsequent dehydration at 70 – 100 km depth weakens the plate due to pore fluid pressure. Even though outer rise seismicity has many important effects on subduction zone processes, the

amount of water in subduction zones, the depths to which water extends in the mantle, and controlling factors for serpentinization in the outer rise are not known for most subduction zones [*Lefeldt et al.,* 2009]. Seismologists have recognized that the maximum depth of extensional brittle faulting in the outer rise commonly corresponds to the depth of mantle serpentinization. Thus recent studies have inferred the depth of mantle hydration by determining the depth of the transition zone, referred to as the neutral plane, from brittle tensional to extensional faulting [*Lefeldt et al.,* 2009; *Emry et al.,* 2014]. This study will focus on the calculation of the depth of outer rise earthquakes of the Nazca plate in the Colombian and Chile subducting regions by the relocation, teleseismic waveform inversion and depth estimation of outer rise earthquakes.

CHAPTER 2: LITERATURE REVIEW

A. The Outer Rise and Plate Stress Field

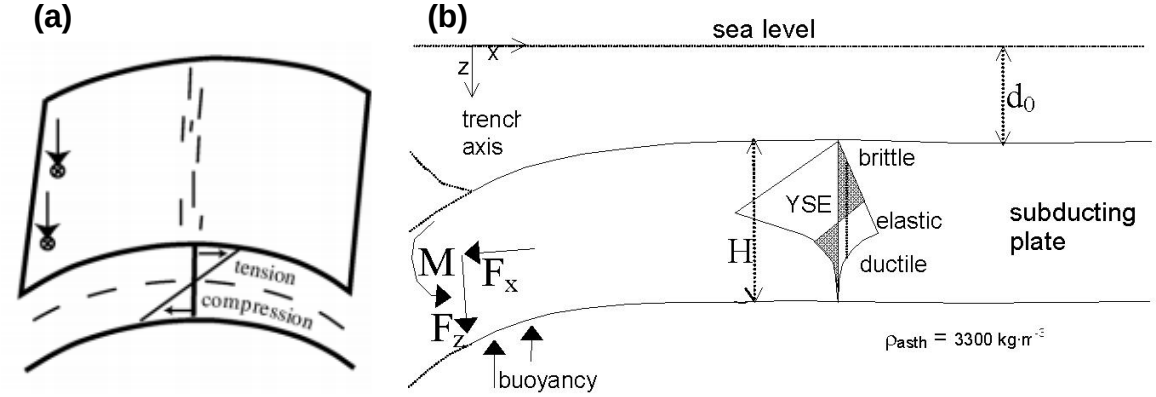

[*Supak et al.*, 2006] [*Garcia- Castellanos et al.*, 2000]

Figure 2.1. (a) Lithospheric flexure model. **(b)**Model of the lithosphere of a subducting plate. Bending is caused by an applied moment, represented as M, and the vertical and horizontal forces Fz and Fx, respectively. The depth of seawater is represented as d_o, and the thickness of the subducting plate is H. The straight lines at the apex of the bend in Figure 2.1a show the stress within the plate material which would rupture during an earthquake. The brittle region in Figure 2.1b makes up approximately the top shallow half of the yield stress envelope (YSE). The ductile region makes up the lower portion of the YSE, where the rocks exhibit ductile deformation.

As a subducting plate approaches the trench, the state of stress within the oceanic lithosphere varies with depth and distance from the trench [*Craig et al.*, 2014]. Plate bending models [e.g. *Chapple and Forsyth*, 1979; *Seno and Yamanaka*, 1996; *Clouard et al.*, 2007] predict that tensional stress is limited to the upper lithosphere, with compressional stress restricted to the deeper region of the plate. Figure 2.1a shows the regions of tension and compression within the bending plate [*Supak et al.*, 2006] and Figure 2.1b shows the zones within the plate that exhibit brittle, elastic, and ductile behavior [*Garcia- Castellanos et al.*, 2000]. Rocks yield in a more brittle manner at lower stresses when under tension than when under compression [*Garcia- Castellanos et al.*, 2000]. The rock behaves elastically wherever the

stress within the material is not large enough to match the brittle or ductile yield stress. Rupture occurs where the shear stress overcomes the frictional stress [G*oetze and Evans,* 1979; *Kirby*, 1980; *Brace and Kohlestedt,* 1980]. The neutral plane is the region of little to no seismicity where the stress field changes from tensional to compressional. The brittle extensional faulting in the upper most oceanic subducting plate (crust and mantle) is where it is proposed that seawater is able to enter the subducting plate, with the neutral plane acting as a barrier for deeper seawater penetration [*Peacock,* 2001; *Ranero et al.,* 2003; *Ranero and Sallares,* 2004].

B. Subduction Zone Water Cycle and Outer Rise Earthquakes

Rüpke et al. [2004] affirm that there is an established connection between the oceans and Earth's water cycle. The effect of localized hydration in subducting oceanic plate lower crust and upper mantle can result in water flux from the subducting slab to the forearc and arc region [*Korenaga,* 2007; *Wada et al.,* 2012], affecting arc and back-arc volcanism [*Gill,* 1981*; Rüpke et al.,* 2004; *Emry et al.,* 2014]. Hydration in the outer rise is also connected to other aspects of Earth's water cycle such as slip along the plate interface, mantle composition and serpentinization, and intermediate depth earthquakes [*Rüpke et al.,* 2004; *Hirschmann,* 2006; *O'Neill et al.,* 2007; *Barcheck et al.,* 2012]. Outer rise tensional normal faulting can possibly cut deep enough into the lithosphere to allow seawater to enter the mantle, changing the peridotites into serpentinites containing up to 13 weight percent water (wt % H_2O) [*Ranero et al.,* 2003; *Peacock,* 2001; *Grevemeyer et al.,* 2007].

Outer rise earthquakes are either shallow normal or deeper thrust or reverse faulting events [*Chapple and Forsyth,* 1979; *Christensen and Ruff,* 1988] that promote hydration of surrounding crust and mantle, providing a potential pathway for seawater to enter the plate [*Ranero et al.,* 2003]. Tensional outer rise events highlight areas of newly created faults or

reactivated faults, and the infiltration of water in the upper lithosphere of the plate [*Ranero et al.*, 2003; *Moscoso and Contreras-Reyes,* 2012]. The neutral plane between tensional seismicity in the upper layers of the plate and compressional seismicity in the lower portion of the plate is possibly a barrier for seawater penetration and the limit of serpentinization [*Lefeldt et al.*, 2009]. Compressional earthquakes occur beneath the neutral plane and are attributed to the compressional bending stresses or in-plane loading caused by plate coupling [*Chapple and Forsyth*, 1979; *Christensen and Ruff,* 1988]. Compressional events occur in much fewer numbers and at deeper depths than tensional earthquakes in the outer rise.

Lefeldt et al. [2009] suggest that outer rise events larger than M_w=5 might create faults that may allow sea water to penetrate the plate down to depths of the earthquake origin. There are numerous events larger than M_w=5 that occur in the outer rise in Colombia, Ecuador, Peru, and Chile, which perhaps contribute to seismicity at deeper depths, bending related faults, and more hydration in the subducting plate than previous studies have predicted [*Van Avendonk et al.*, 2011].

Other than high lithostatic pressure, it is not certain how or by what process water is pulled to depth. However, some studies suggest that plate bending causes tectonic pressure gradients within the upper oceanic lithosphere that pull water into the mantle [*Faccenda et al.*, 2009; *Emry et al.*, 2014]. If serpentinization occurs along outer rise faults, then the amount of water within the oceanic plate mantle is possibly equal to the amount of water stored within the oceanic crust [*Ranero et al.*, 2003; *Emry et al.*, 2014].

The Earth's water cycle consists of the hydration and dehydration of subducting oceanic lithosphere. Water is chemically bound within the incoming plate's sedimentary, crustal, and mantle portions [*Rüpke et al.*, 2004]. The shallowest dehydration is < 20 km depth and consists

of expelled water from pore and structurally-bound water in subducting sediments [*Jarrard*, 2003; *Rüpke et al.*, 2004; *Emry et al.*, 2011]. Water expelled within the upper crustal layer down to 50 km depth is the stage of the water cycle that may affect plate interface slip and other shallow subduction zone processes [*Jarrard*, 2003; *Shelly et al*., 2006; *Audet et al*., 2009; *Emry et al*., 2014]. In intermediate depth dehydration (50 - 100 km), water expels from the lower crustal layer and upper mantle serpentinites [*Jarrard*, 2003; *Van Keken et al.*, 2011] and affects volcanic arc output and back arc basin output [*Gill*, 1981; *Kelley et al.*, 2006]. At depths down to 100 km, the de-serpentinization of the mantle triggers arc melting [*Rüpke et al.*, 2004].

Hydration in the outer rise has been suggested to occur more commonly in subduction zones with relatively fast convergence and brittle subducting oceanic crust [*van Keken et al.*, 2011]. *Emry et al.* [2014] observed that the maximum centroid depth of tensional earthquakes in the central Marianas was on the order of 11 km below the Moho, which agreed with models of serpentinized mantle depth. Such a model as that of *Emry et al*. [2014] suggests that the overall hydration in the Marianas is much greater than other models have predicted. The Mariana subduction zone, like the Nazca subduction zone, is a highly coupled region with relatively fast subduction. However, in contrast to the old (~170 million years), thick, and cold Pacific plate in the Mariana subduction zone, the Nazca plate has relatively young oceanic lithosphere (~ 20 - 40 million years) and subduction dip varies between 9° -30° along the length of the plate [*Gutscher et al.*, 2000; *Garcia et. al.*, 2007]. Thus, we expect the depth of tensional faulting and hydration in the Nazca outer rise to be more shallow than in the Marianas outer rise.

C. Structure of the Nazca Plate Offshore South America

The state of stress and hydration is not well constrained for the Nazca - South American plate subduction zone, specifically offshore Colombia and the 4,270 km extent of offshore Chile. The convergence rate of the Nazca plate with South America also changes throughout this subduction zone, increasing from 6.0 *cm/yr* at ~ 5°N to 7.0 *cm/yr* at ~ 5°S to 7.8 cm/yr at ~ 15°S to 8.4 *cm/yr* at ~ 30°S [*Gutscher et al.,* 2000]. There is no linear relationship between latitude and the age of plate. *Gutscher et al.* [2000] estimated that the age of the subducting Nazca plate varies from ~ 22 Ma, 12 Ma, 43 Ma, and 6 Ma [*Tilmann et al*., 2008] at 7°N, 4.5°N, 24°S-31°S, and 41°S, respectively. There are multiple fracture zones (oblique and perpendicular to the trench), multiple transform faults, the Sandra rift (no longer spreading) perpendicular to the trench, as well as the Carnegie, Nazca, Iquique, and Juan-Fernandez ridges [*Gutscher et al.,* 2002]. Pre-existing fractures associated with features in the bathymetry (such as ridges and seamounts) could be a controlling factor in the nucleation of outer rise seismicity [*Fromm et al.,* 2006]. As seen in Figure 2.2, there are large concentrations of outer rise normal faulting events in the Colombia and Chile regions (8°N - 0°N and 22°S - 46°S). Additionally there are regions with lower rates of earthquakes along the margin (0°N - 5°S and 12°S - 25°S).

The seafloor structure is unusual in the northern part of the study region of 8°N - 0 °N. From 5.6°N - 7°N, the subduction is characterized by shallow, flat- slab subduction of the Panama Basin, with no volcanic arc [*Gutscher et al.,* 2000]. The presence of volcanic arcs affirm that there is water in the Nazca plate. There is a volcanic gap from 2°S - 15°S, possibly due to flat slab subduction [*Gutscher et al.,* 2000].

At 15°S latitude and farther south to 45° S, the character of subduction changes, with a steep subduction angle and the presence of a volcanic arc [*Gutscher et al.,* 2000]. The

concentration of normal faulting outer rise events in Chile correlates with regions seaward of rupture from the 1960 M_w=9.5 Valdivia and 2010 M_w=8.8 Maule megathrust earthquakes [*Craig et al.,* 2014]. As a result, this study will concentrate on these areas along the 1960 and 2010 rupture areas.

Figure 2.2 also displays the areas of volcanic arcs (8°N - 2°S, 15°S - 27°S, and 32°S - 46°S) and gaps (5°S - 15°S and 27°S - 32°S) along the margin of the Nazca plate. These volcanic arcs and gaps could possibly be related to plate hydration in the outer rise because of water's effect to lower the mantle melting temperature [*Gutscher et al.,* 2000; *Emry et al.,* 2011]. In the Chile subduction zone near 32°S, the outer rise seismicity may be influenced by the complex fault system created by the subduction of the Juan Fernandez Ridge [*Clouard et al.,* 2007; *Fromm et. al.,* 2006].

In the southern portions of South America, extending throughout southern central Chile (41-44°S), the plate is older (15-25 Ma) and therefore relatively colder and more rigid than younger portions of the plate. There is approximately 9% hydrated (serpentinized) lithosphere in the upper 2 km of the Nazca plate [*Contreras -Reyes,* 2007], but hydration and dehydration of the subduction zone of Colombia is not well known or investigated [*van Keken et al.,* 2011].

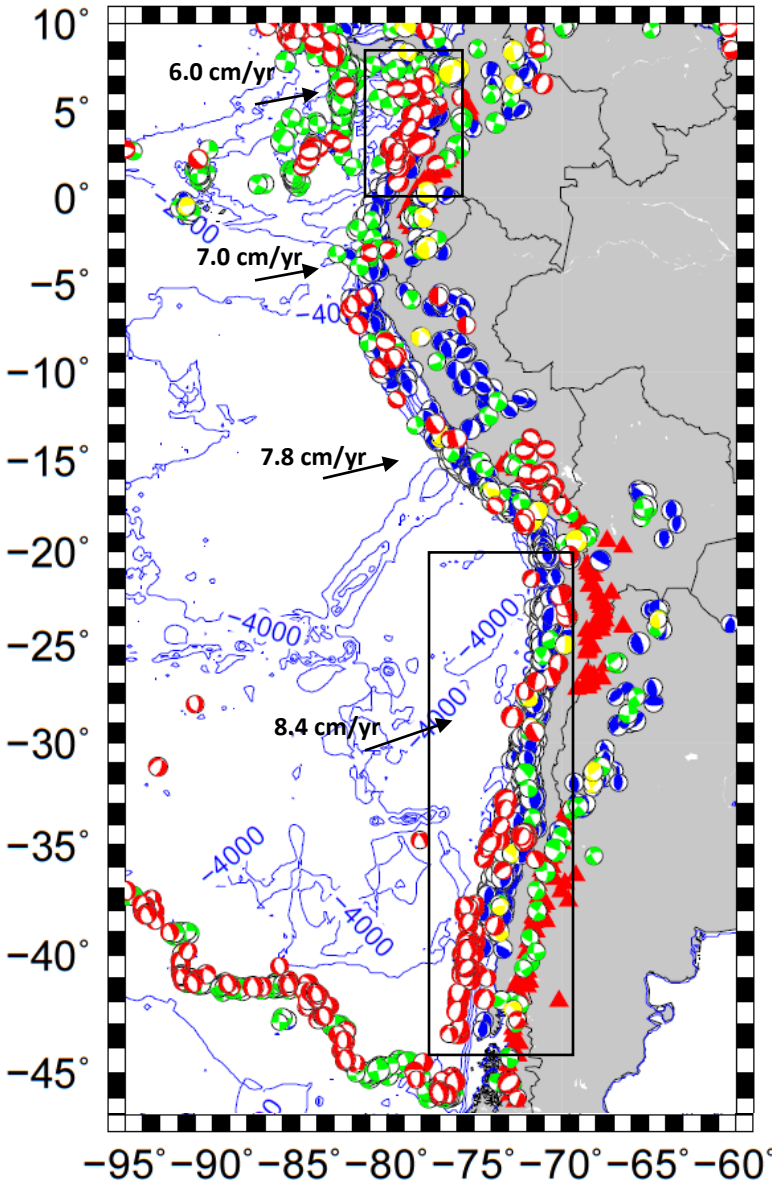

Figure 2.2. Plot of the west South American coast with Global Centroidal Moment Tensor (GCMT) catalogue earthquakes from 1976 to 2013 with depths < 50 km. The red focal mechanisms represent normal faulting earthquakes. Normal faults are typical of outer rise events [*Grevemeyer et al.*, 2005, 2007]. Thus, the clusters of red focal mechanisms identify areas that have significant outer rise seismicity. The blue contour lines show depth to the seafloor, drawn at 1000 m intervals. The red triangles represent volcanoes. Thrust, oblique, and strike slip events are blue, yellow, and green respectively. The boxed in regions are the areas of study.

D. Previous Studies of the Nazca Plate Outer Rise

In previous studies, the subducting mantle off the coast of Nicaragua (north of this paper's study area) is suggested to be about 20 - 30% serpentinized. *Lefeldt et al.* [2009] inferred the depth of the neutral plane in the Nicaraguan outer rise from earthquake focal mechanisms and found that it corresponded to a region of low P-wave velocities, characteristic of mantle serpentinization. In the Nicaraguan outer rise, serpentinization occurs down to a depth of 5 - 10 km with plate hydration of 3 - 4 wt % H_2O [*Van Avendonk et al.*, 2011]. The results from *van Keken et al.* [2011] suggest that the Colombia and Peru regions have less water input. The Chile region has similar water input to that of Nicaragua, though the entire region from Colombia to Chile has much more dehydration, which occurs at ~100 km depth, throughout the subduction process [*Van Avendonk et al.*, 2011; *van Keken et al.* 2011].

Both *Clouard et al.* [2007] and *Fromm et al.* [2006] studied the 04/09/2001 outer rise Chile earthquake, which is the largest outer rise event, ($M_W = 7.0$) [*Fromm et al.*, 2006], to have occurred since 1993 in the study region. This earthquake was calculated by both studies to have a source depth of ~12 km. Both concluded that the outer rise earthquake was characterized by normal faulting, striking sub-parallel to the Juan Fernandez Ridge and could have created faults that allowed seawater into the plate. Both studies also mention that the nearby O'Higgins fracture zone and the Juan Fernandez Ridge affect outer rise seismic nucleation [*Fromm et al.*, 2006; *Clouard et al.*, 2007]. *Clouard et al.* [2007] inferred that the lithosphere in this region of Chile is in tension down to a depth of 30 km and *Fromm et al.* [2006] inferred that brittle failure occurs from 10 - 30 km depth.

Oceanic intraplate seismicity is confined to regions colder than 600° C [*McKenzie et al.*,2005; *Craig et al.*, 2014]. The 600° C isotherm in the Central American outer rise has been

inferred to be at 18 - 26 km depth with the deepest extensional earthquake at 10 km and deepest compressional earthquake at 15 km [*Craig et al.*, 2014], which agrees with the *Van Avendonk et al.* [2011] study. The aseismic region corresponding to the 600° C isotherm in the Chile outer rise has been inferred to be at 15 - 35 km depth, with the deepest extensional and compressional earthquakes at 23 km and 28 km depths, respectively [*Craig et al.*, 2014]. This would suggest a neutral plane at 24 - 27 km depth for the Chile outer rise. However, the *Craig et al.* [2014] study assumed a uniform curvature structure of the Nazca plate, which in reality has bathymetry and curvature that varies greatly along the length of the Chile subduction zone.

CHAPTER 3: EARTHQUAKE RELOCATION

A. Data and Methods

Uncertainties in automated teleseismic event locations, especially for shallow earthquakes, can be caused by timing errors, the limitations of the algorithms, or phase pick errors [*Lomax et al.*, 2000; *McGinnis*, 2001]. Therefore, relocation is necessary to have accurate event epicenter locations and to distinguish the outer rise earthquakes from shallow thrust earthquakes in the forearc of the subduction zone [*Emry*, 2011]. In this research, we used the hypocentroidal decomposition method [*Jordan and Sverdrup*, 1981] to precisely locate outer rise earthquake epicenters in the study area down to a depth of 50 km. We identified earthquakes with depths < 50 km and MW≥ 5 for the Colombia region (0°N - 10 °N, 77°W - 83°W) and MW≥ 5.5 for the Chile region (18°S - 44°S, 72°W - 82°W) from 01/01/1976 to 01/01/2013 in the Global Centroidal Moment Tensor (GCMT) catalogue [*Ekström et al.*, 2012]. Arrival time data was collected from the International Seismic Center (ISC) Bulletin, including P, pP, PKP, and S phases for earthquakes MW≥ 5, for the Colombia and Chile regions. Earthquakes >80 km landward of the trench are excluded. The remaining GCMT earthquakes were combined with arrival time data for the same events.

The hypocentroidal decomposition algorithm [*Jordan and Sverdrup*, 1981] was used to calculate more accurate locations than those reported in the ISC Bulletin. The *Jordan and Sverdrup* [1981] method is dependent on the assumption that if the distance between earthquake hypocenters is small, then the difference in travel times to a station does not include the effects of velocity heterogeneity [*Wolfe*, 2002]. This method relocates earthquakes within a cluster with respect to the cluster centroid by projecting out the part of the travel-time deviations that are

common to particular stations [*Shearer*, 2009]. Earthquake ISC and GCMT earthquake locations were separated into two regions of Colombia (0°N - 10 °N) and Chile (18°S - 44°S).

B. Results - Colombia

In Colombia, relocation was done in one section since the study region is relatively small, 0° - 10°N, and the ray paths should be similar throughout this section. Of the initial 42 GCMT events, 38 had ISC arrival time data available and thus 38 events were relocated. Table 3.1 compares GCMT and relocated latitudes and longitudes (epicenters) for all earthquakes used in the relocation.

Table 3.1. Earthquake GCMT and Relocated Epicenters for Colombia

Event #							GCMT		Relocated	
	Year	mo	day	hr	mn	sec	Lat°	Lon°	Lat°	Lon°
1	1978	2	16	3	47	24.7158	5.84	-78.24	5.4568	-77.6556
2	1979	12	13	2	43	37.1670	5.66	-80.46	5.5014	-80.5307
3	1979	12	13	5	37	52.9961	2.88	-79.49	2.5467	-79.6342
4	1979	12	31	23	7	25.4375	1.93	-79.71	2.0712	-79.0368
5	1980	1	7	0	33	39.0885	2.74	-79.06	2.8787	-78.7466
6	1980	1	26	15	27	16.0000	2.52	-79.84	2.3341	-79.3804
7	1980	5	11	9	25	59.9688	1.95	-80.32	1.7889	-80.4094
8	1981	1	7	7	1	41.5059	1.72	-79.31	2.0136	-79.2436
9	1981	7	7	10	25	46.8438	2.77	-79.87	2.7373	-79.8203
10	1982	3	16	8	4	56.3281	6.26	-78.65	5.8299	-78.2359
11	1982	8	1	20	38	17.4375	2.71	-79.40	2.5268	-78.8939
12	1984	7	30	4	27	28.6846	2.58	-79.35	2.2749	-78.9946
13	1985	6	10	3	23	34.1133	3.24	-78.99	3.0316	-78.5034
14	1987	1	13	13	23	57.2031	5.68	-78.90	5.7464	-79.0461
15	1987	1	13	19	30	13.7109	5.87	-78.86	5.6232	-78.8854
16	1987	1	25	10	31	23.9883	3.30	-79.31	3.0637	-79.3184
17	1988	9	20	17	56	20.4688	4.99	-77.68	4.7097	-77.3646
18	1989	1	17	11	20	47.4609	5.93	-79.01	5.6492	-79.1387
19	1989	2	12	20	3	17.7891	2.41	-79.44	2.6994	-79.8594
20	1989	9	9	1	40	39.1587	1.92	-79.53	2.5003	-79.7493
21	1990	8	25	11	43	29.0352	5.71	-77.93	5.6696	-77.5470
22	1990	8	25	11	47	35.4297	6.26	-77.63	5.7542	-77.4348
23	1994	9	27	23	4	50.2266	5.90	-78.92	5.7212	-79.1836
24	1994	11	26	4	48	7.5859	2.65	-79.32	2.8374	-79.5167
25	1995	4	13	15	0	34.5234	5.29	-79.80	5.5164	-79.8747
26	1996	4	27	8	40	44.6113	2.47	-79.42	2.3983	-79.3764
27	1997	9	9	5	45	48.9727	5.47	-77.82	5.8313	-77.4338
28	2000	3	19	12	23	39.7109	5.69	-77.61	5.6210	-77.5754
29	2000	7	12	22	12	14.8906	6.54	-77.80	6.2713	-77.6495
30	2002	8	8	13	39	58.9688	5.17	-77.62	5.1058	-77.7542
31	2002	12	21	0	46	12.1624	3.76	-78.90	3.8016	-78.9008
32	2003	11	5	0	58	45.1602	5.14	-77.81	5.0239	-77.5594
33	2004	1	12	14	14	30.6328	5.76	-79.08	5.7205	-79.1646
34	2007	3	17	22	43	10.1875	4.61	-78.53	4.6504	-78.4788
35	2007	3	18	2	11	7.5259	4.69	-78.53	4.7135	-78.4477
35	2010	8	21	20	20	16.7656	6.08	-78.04	6.0669	-77.9800
37	2011	9	13	4	38	46.9570	5.77	-77.75	5.6601	-77.5544
38	2011	9	13	4	49	35.9395	5.73	-77.66	5.6660	-77.5358

As shown in Figure 3.1, earthquake relocations appear to have no pattern or general trend of the location change, which suggests there was no systematic bias in the catalogue locations. The differences in latitude and longitude ranged from 0.04 - 0.4°.

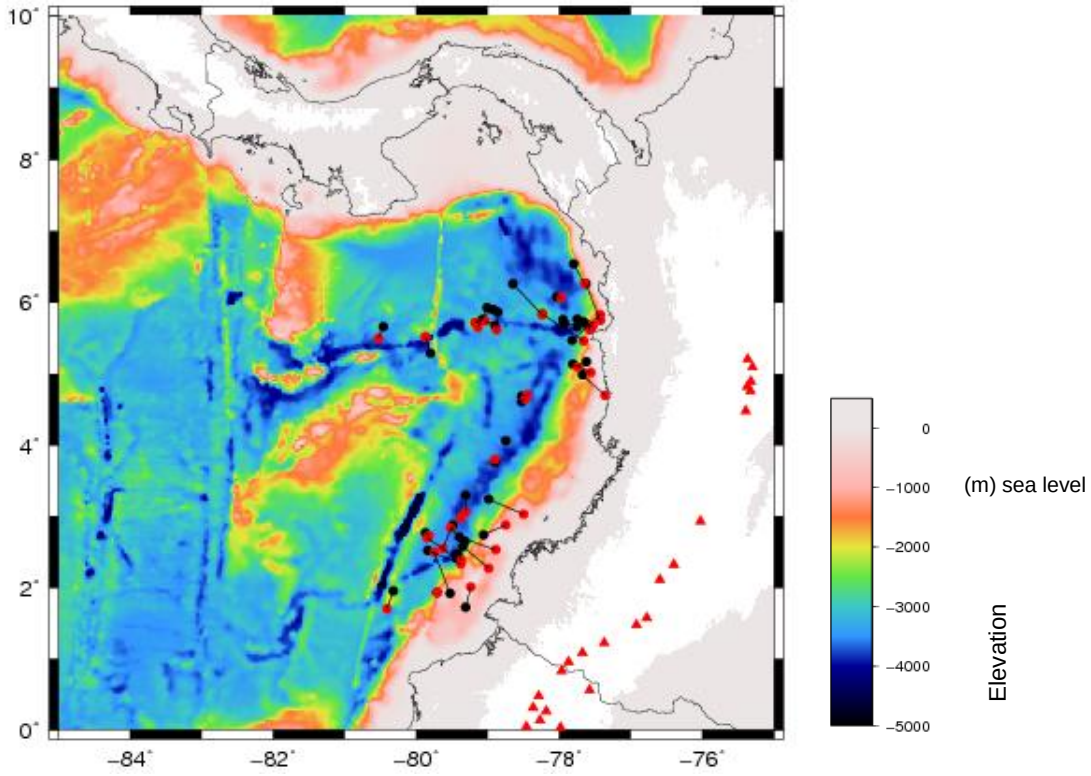

Figure 3.1. Initial GCMT and relocated events. Plot of the GCMT earthquake epicenters (black points) connected with a black line to relocated earthquakes (red points) occurring in the region from 8°N - 0 °N and depth < 50 km, from 1976 to 2013. The red triangles represent volcanoes.

C. Results - Chile

The same procedure as was applied to the dataset of Colombia was applied to the Chile dataset. However, since the velocity structure of the Earth can vary significantly, even along the same subducting plate, the Chile relocation was done in four almost equally sized latitude sections so the clusters of earthquakes in each section have similar source-receiver paths. The four relocation regions were divided thusly: 18°S - 27°S, 27°S - 33°S, 33°S - 38°S, and

38°S - 44°S. Note that the two northernmost of these regions had few earthquakes. Thus, earthquakes occurring > 80 km seaward of the trench were included, and the earthquakes from section 2 were combined with section 1 in order to have at least 15 events for each relocation section. The sections that relocation was done are shown in white boxes in Figure 3.2. Of the initial 79 GCMT events in Chile, 65 earthquakes were relocated. The results of the earthquake relocation is listed in Table 3.2. Like Colombia, there appears to be no pattern or general trend of the change earthquake location (Figure 3.2).

Table 3.2. Earthquake GCMT and Relocated Epicenters for Chile

Event #							GCMT		Relocated	
	Year	mo	day	hr	mn	sec	Lat°	Lon°	Lat°	Lon°
1	1976	2	28	16	27	13.1797	-40.00	-74.73	-39.9404	-74.9379
2	1976	5	30	3	8	54.7227	-41.64	-75.41	-41.5260	-75.3552
3	1980	5	30	16	56	22.4297	-23.11	-70.93	-23.1413	-70.7933
4	1980	3	29	6	41	50.7305	-43.08	-75.20	-42.9955	-75.3616
5	1981	10	16	3	25	41.5039	-33.13	-73.07	-33.2108	-73.0705
6	1982	6	1	4	14	16.7383	-41.63	-74.99	-41.4574	-75.0702
7	1982	6	5	0	17	3.4730	-43.10	-75.21	-42.9522	-75.1670
8	1983	5	9	10	58	26.6055	-40.87	-74.84	-40.9493	-74.9703
9	1984	4	19	8	28	53.2832	-31.80	-71.90	-31.8602	-71.8901
10	1985	4	28	8	30	34.6973	-39.70	-75.61	-39.6395	-75.7667
11	1985	11	6	16	8	52.9766	-40.62	-74.87	-40.7975	-75.0092
12	1987	3	10	0	22	35.9125	-18.53	-72.15	-18.4157	-72.0020
13	1987	1	27	7	6	52.7168	-32.13	-72.04	-32.1297	-72.0240
14	1987	5	19	12	56	26.4336	-30.33	-71.59	-30.3341	-71.4491
15	1988	3	13	11	31	34.0039	-33.67	-72.27	-33.5331	-72.2072
16	1989	4	13	0	43	10.6016	-39.56	-75.03	-39.3898	-74.9873
17	1990	8	2	5	24	9.5469	-31.61	-71.58	-31.6425	-71.7627
18	1992	11	4	21	32	37.1484	-31.63	-71.55	-31.6305	-71.6026
19	1992	11	28	3	13	34.8926	-31.40	-71.94	-31.3757	-72.0410
20	1994	9	17	12	22	16.3438	-32.19	-71.67	-32.2715	-71.8404
21	1995	10	3	16	8	17.964	-30.74	-71.97	-30.7038	-71.9435
22	1996	2	19	7	10	9.6191	-42.09	-75.08	-42.0793	-75.3099
23	1997	7	6	9	54	0.6836	-30.06	-71.87	-30.0906	-71.9150
24	1997	7	6	23	15	20.9453	-30.16	-71.86	-30.1625	-71.9429
25	1997	7	19	12	2	59.1055	-29.28	-71.68	-29.2999	-71.6694
26	1997	7	24	19	54	35.7031	-30.58	-72.02	-30.5655	-72.1070
27	1997	7	25	6	47	1.4941	-30.46	-71.91	-30.4470	-72.0396
28	1997	7	27	5	21	31.9316	-30.52	-71.86	-30.4885	-71.9210
29	1997	8	18	12	24	25.4688	-29.93	-72.01	-29.8608	-71.9930
30	1998	4	1	22	43	0.4844	-40.32	-74.87	-40.3434	-75.0201
31	1999	9	29	18	1	33.3594	-30.74	-71.99	-30.6992	-71.8924
32	2000	12	20	11	23	52.6602	-39.01	-74.66	-39.0725	-74.9239
33	2001	4	9	9	0	58.1289	-32.67	-73.11	-32.7825	-73.4024
34	2001	3	3	11	58	2.9063	-38.77	-74.56	-38.9114	-75.0435
35	2003	11	12	1	54	24.3589	-40.02	-74.87	-39.9831	-74.9425
36	2003	2	20	20	7	5.3906	-18.44	-70.99	-18.4071	-70.9302
37	2003	6	19	23	4	59.7344	-30.69	-71.54	-30.6826	-71.6268
38	2004	1	19	5	47	24.4824	-31.73	-71.72	-31.7049	-71.6690
39	2004	4	3	9	57	13.8125	-29.99	-71.99	-29.9769	-71.9410
40	2004	9	27	22	58	25.8906	-32.69	-71.74	-32.6172	-71.6131
41	2005	3	1	7	24	5.7578	-31.43	-71.69	-31.4247	-71.6698

Table 3.2 Continued

Event #							GCMT		Relocated	
	Year	mo	day	hr	mn	sec	Lat°	Lon°	Lat°	Lon°
42	2006	4	15	23	50	13.2813	-29.77	-72.00	-29.6107	-71.8641
43	2006	7	16	11	42	40.6680	-28.72	-72.54	-28.6865	-72.5420
44	2006	10	12	18	5	58.6602	-31.30	-71.33	-31.2441	-71.3701
45	2006	5	25	20	48	5.0859	-18.14	-71.16	-18.0835	-71.1047
46	2007	3	29	14	40	42.7031	-31.59	-71.84	-31.5669	-71.7569
47	2007	3	29	17	9	2.6797	-31.60	-71.71	-31.5637	-71.7217
48	2007	12	15	18	22	28.4531	-32.69	-71.68	-32.7007	-71.6246
49	2007	12	20	3	6	57.0732	-32.71	-71.79	-32.6921	-71.6267
50	2008	12	18	21	19	32.4766	-32.46	-71.73	-32.4173	-71.6819
51	2008	12	18	21	50	29.3672	-32.47	-72.05	-32.4642	-71.6653
52	2008	12	19	7	30	10.0645	-32.54	-72.02	-32.5572	-71.9160
53	2008	12	19	9	36	8.1914	-32.46	-71.95	-32.4261	-71.7607
54	2009	11	22	22	7	51.0391	-39.64	-74.97	-39.6120	-74.9703
55	2010	3	1	7	49	11.1270	-34.71	-73.12	-34.6651	-73.2802
56	2010	3	2	6	10	56.0742	-34.53	-72.68	-34.5108	-72.7065
57	2010	3	10	12	20	59.1602	-33.56	-72.30	-33.5775	-72.3801
58	2010	10	21	2	50	0.6182	-34.74	-73.72	-34.7048	-73.7885
59	2010	12	13	18	51	5.7500	-33.99	-73.08	-33.9884	-73.2730
60	2010	4	16	22	41	40.3359	-37.57	-74.15	-37.4643	-73.6716
61	2010	4	16	23	15	37.9453	-37.65	-74.52	-37.4578	-73.7531
62	2010	4	19	7	32	49.8691	-37.52	-73.68	-37.5459	-73.8581
63	2010	6	28	0	59	50.7629	-37.91	-75.04	-37.7956	-75.1423
64	2011	4	22	5	12	51.4707	-37.90	-73.90	-37.9031	-73.8193
65	2012	10	15	21	4	21.5078	-31.81	-71.79	-31.7966	-71.8813

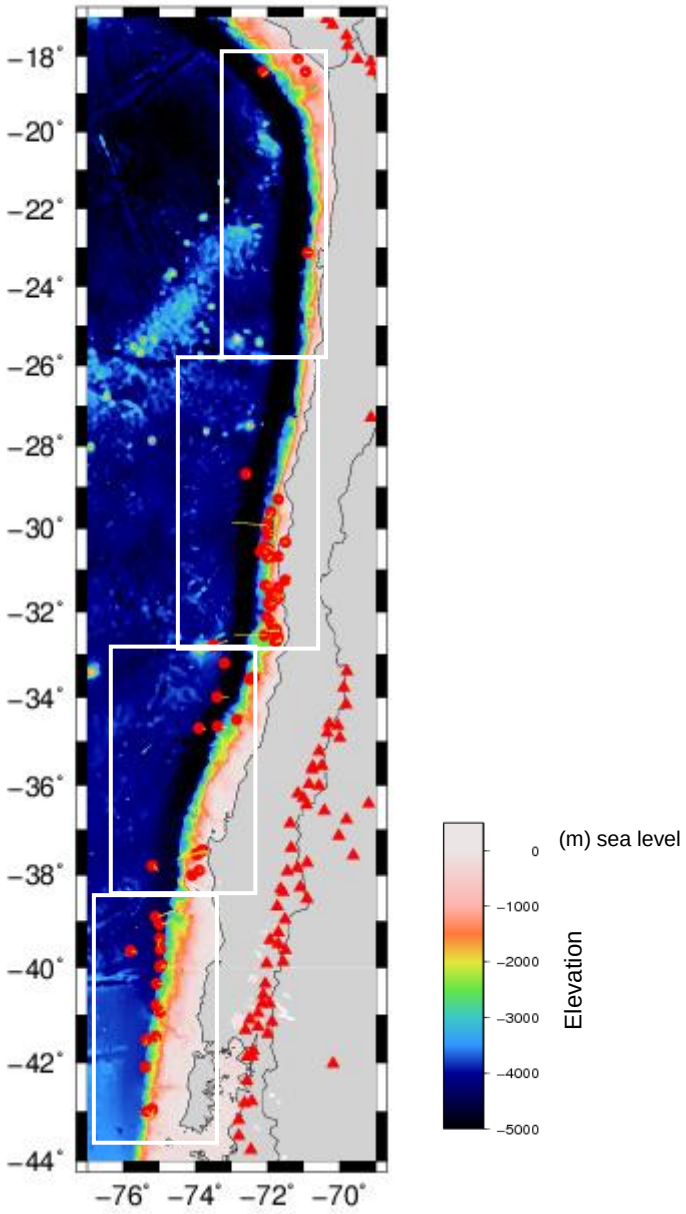

Figure 3. 2. Initial GCMT and relocated events: Plot of relocated epicenters (red) with a yellow line showing the difference of points from the GCMT earthquake locations from 1976 to 2013. The red triangles represent volcanoes. Boxed in regions are the four sections for which relocation was done.

CHAPTER 4: WAVEFORM INVERSION

A. Earthquake Selection and Data

The purpose of performing waveform inversion is to determine the best fitting source parameters for earthquakes located on the incoming plate or near the trench axis. These source parameters include focal mechanism (strike, dip, slip), magnitude, and point source depth. Earthquakes occurring in 1993 or later are those with digital teleseismic waveform data available. The events that have $M_w < 5.50$ are likely to be more susceptible to error due to the smaller magnitudes, shallow source depths and therefore less pronounced wave arrivals. Waveforms were visually inspected for clear signals and teleseismic P-, SH- and SV- waveforms were inverted from stations at distances $30° - 95°$.

Of the 38 relocated earthquakes in the Colombian region, 11 occurred in 1993 or later with a moment magnitude larger than 5.50. Additionally, of the 11 events that occurred in 1993 or later with $M_w \geq 5.50$, only two earthquakes are in the outer rise zone seaward of the trench. These earthquakes are the two largest and most recent events (03/17/07 and 03/18/07, $M_w = 6.00$ and 6.40, respectively). Since there were only two earthquakes in the Colombia region that fit the parameters for waveform inversion, the outer rise events of 11/26/94 and 12/21/2002, both with $M_w = 5.28$, were included in the waveform inversion. Of the relocated earthquakes in the Chile region, 16 occurred in 1993 or later with $M_w \geq 5.50$. Of these 16, 10 were normal faulting events in the outer rise. The relocated events that were used for waveform inversion are plotted for both the Chile and Colombia regions in Figure 4.1.

Broadband teleseismic waveforms were requested from the Incorporated Research Institutions for Seismology (IRIS) Data Management Center (DMC) for the relocated earthquakes $M_w \geq 5.50$ that occurred in 1993 or later and within the region of the outer rise (seaward of the trench, or in close proximity to the trench).

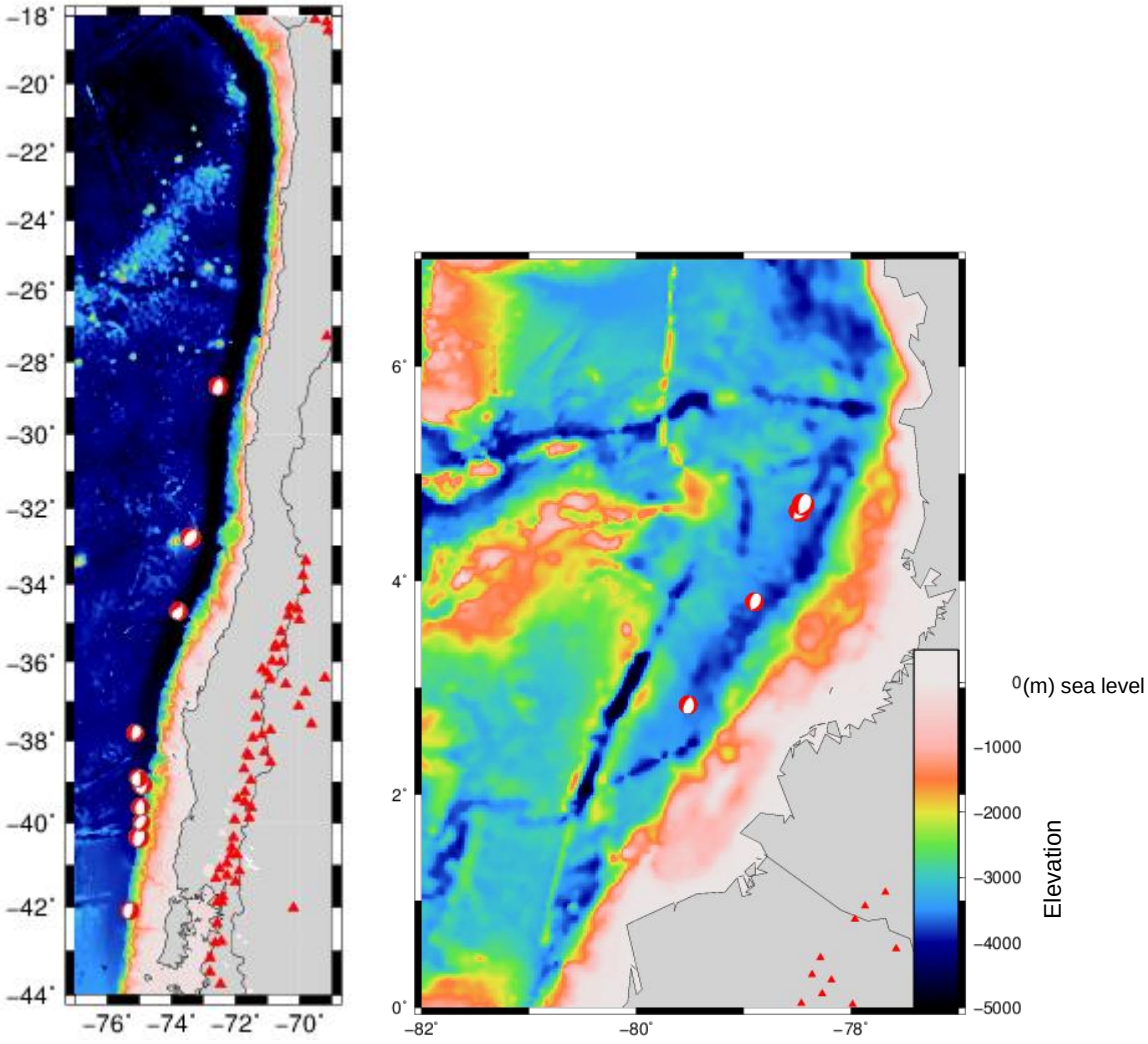

Figure 4.1. Relocated earthquakes used for waveform inversion. The red focal mechanisms represent normal faulting and the red triangles are volcanoes. (**Left)** Chile. **(Right)** Colombia.

B. Method

The vertical component P, transverse component SH, and radial component SV were used for waveform inversion [*Herrmann*, 2013] to determine the best fitting source parameters for earthquakes in the outer rise. Using the teleseismic waveform inversion method [*Herrmann*, 2013], teleseismic P, SH and SV wave signals were inverted to derive source depth and focal mechanisms using different and separate earth velocity models for the source-side and receiver-side structures [*Hudson*, 1969; *Herrmann*, 1976, 2013]. The computation of the overall fault mechanism and depth of a single point source represents the onset time and the depth [*Lefeldt and Grevemeyer*, 2008]. The method uses Green's functions (the impulse response of a medium) to make synthetic seismograms which are then compared to the observed seismograms [*Herrmann*, 1976]. The synthetic waveforms that match the observed waveforms the best will determine the more accurate depths. In the general case of Green's function method, a moment tensor with six independent elements is used to describe the point source. When the synthetic and observed waveforms are highly correlated, the calculation of the overall focal mechanism of the earthquake will determine the locations (depth) of the point sources of the events [*Kikuchi and Kanamori*, 1991].

Predicted or synthetic seismograms y(t) are determined by the following equation:

$$y(t) = s(t) * R_{sc}(t) * M(t) * R_{rc}(t) * I(t)$$

where,

$s(t)$ = Source time function of double couple without moment force system
$R_{rc}(t)$ = Response at surface of the receiver crust for an incident impulsive teleseismic P wave
$R_{sc}(t)$ = Source crust response
$I(t)$ = Impulse response of the seismograph system used

$M(t)$ = Mantle impulse response for P waves

$$M(t) = G(\Delta)Q(t)$$

where,

$G(\Delta)$ accounts for geometric spreading within mantle upon the amplitude of the P-wave
Δ = epicentral distance from source to receiver or station

[*Herrmann*, 1976]

The waveform inversion was computed with source-side velocity models [*Hudson*, 1969] with water layers of 0, 3.5 and 4 km thickness, all with P-velocity of 1.8 km/s for the water layer and almost zero shear modulus (0.0001 Pa) and S-velocity (0.0001 km/s). These models also incorporated a sediment layer of 0.64 km to make the model as close to realistic seafloors of Chile and Colombia as possible [*Herrmann*, 1976]. The Green's functions were created using the program hudson96 [*Hudson*, 1969; *Herrmann*, 2013] for those source-side models. The receiver-side model has a simple continental crust model [*Herrmann*, 2013]. The velocity model for the source-side with 4.0 km water layer is listed below in Table 4.1, and the velocity model for the receiver-side continental model is shown in Table 4.2.

Table 4.1. Source-side 4.0 km water layer velocity model. Thickness of layer, P- and S-wave velocities, density, P and S attenuation are represented as H, VP, VS, RHO, QP, and QS.

ISOTROPIC
SPHERICAL EARTH
1-D

H(KM)	VP(KM/S)	VS(KM/S)	RHO(GM/CC)	QP	QS
4.0000	1.8000	0.0001	1.0290	0.323E-02	0.667E-02
0.6400	1.8000	0.3000	2.1000	0.323E-02	0.667E-02
5.0000	6.5000	3.8500	2.9200	0.123E-02	0.250E-02
11.5000	8.0425	4.4850	3.3326	0.128E-02	0.292E-02
15.0000	8.0425	4.4850	3.3326	0.128E-02	0.292E-02
0.5000	8.0425	4.4850	3.3326	0.128E-02	0.292E-02
24.5000	8.0425	4.4850	3.3326	0.128E-02	0.292E-02
17.5000	8.0425	4.4850	3.3326	0.128E-02	0.292E-02
0.5000	8.0425	4.4850	3.3326	0.128E-02	0.292E-02
22.0000	8.0475	4.4950	3.3584	0.180E-02	0.417E-02
20.0000	8.0475	4.4950	3.3584	0.180E-02	0.417E-02
0.5000	8.1123	4.5045	3.3990	0.855E-02	0.131E-01
44.5000	8.1123	4.5045	3.3990	0.855E-02	0.131E-01

Table 4.2. Receiver-side continental model used for all waveform inversions. Thickness of layer, P- and S-wave velocities, density, P and S attenuation are represented as H, VP, VS, RHO, QP, and QS. Note that not all the rows of the table are shown. Layers of ~50 km depth are continued with nearly constant values of VP, VS, RHO, QP and QS till a depth of 770 km is reached in the complete table.

ISOTROPIC
SPHERICAL EARTH
1-D

H(KM)	VP(KM/S)	VS(KM/S)	RHO(GM/CC)	QP	QS
20.0000	5.8000	3.4600	2.7200	310.	150.
15.0000	6.5000	3.8500	2.9200	814.	400.
42.5000	8.0425	4.4850	3.3326	783.	343.
42.5000	8.0475	4.4950	3.3584	555.	240.
45.0000	8.1123	4.5045	3.3990	117.	76.3
45.0000	8.2374	4.5137	3.3477	122.	77.9
50.0000	8.3905	4.5634	3.3453	213.	135.
50.0000	8.5726	4.6525	3.3886	218.	138.
50.0000	8.7553	4.7394	3.4344	224.	141.
50.0000	8.9380	4.8263	3.4822	231.	145.
50.0000	9.4433	5.1330	3.9295	259.	164.
50.0000	9.6114	5.2388	3.9253	261.	166.
50.0000	9.7794	5.3450	3.9225	263.	168.
50.0000	9.9473	5.4513	3.9212	265.	170.
50.0000	10.1153	5.5570	3.9204	267.	172.
50.0000	10.8562	6.0246	4.2687	837.	546.
50.0000	10.9883	6.1493	4.3275	818.	541.

The observed and Green's function waveforms were corrected for instrument response to ground velocity in m/s for the passband of 0.004 - 5 Hz. The traces were then lowpass filtered below 0.25 Hz and interpolated to a sample interval of 1 second [*Herrmann*, 2013]. To reduce the sensitivity to the source duration, a bandpass filter of 0.0167 - 0.0833 Hz is used for events with $M_w < 6.40$, 0.0100 - 0.0500 Hz for events $6.40 \leq M_w < 6.80$, and 0.0083 - 0.0250 Hz for events $6.80 \leq M_w < 7.20$ in the initial waveform inversion with continental model.

The inversion program [*Herrmann*, 2013] is run with a source-side and receiver side continental model first to generate the initial synthetic waveforms. After the program has its initial run, the source-side models are changed to include the water layer. However, in order to have sharper and more recognizable peaks of the phase arrivals, the bandpass filter was extended to include higher frequencies (0.0167 - 0.2 Hz) instead of (0.0167 - 0.0833 Hz) for $M_w < 6.40$. (Most of the earthquakes in this study have magnitudes $M_w < 6.40$.) This enabled us to have better picks for the P-arrival for depth determination but it also led to poorer fit for the waveform

inversion compared to the continental crust source model. The worse fit is most likely due not only to the higher frequencies but also from using a source-side model with water table, which has the effect of reverberations directly following the P-arrival [*Herrmann*, 1976].

Crustal inhomogeneities such as a water layer can cause complex scattering effects in the seismic record, making it difficult to determine focal depth. In order to further constrain the depth and check the depth calculated by the waveform inversion, teleseismic P-wave synthetics from the waveform inversion were used for stations with good signal-to-noise ratios and clear P-wave arrivals. The source parameters inputted are seismic moment, focal depth, strike, dip, rake, and event duration of the triangular shaped source time function [*Herrmann*, 1976]. The observed P-wave signal was plotted with and compared to synthetic waveforms for various focal depths (5-25 km). The best depth was determined by observation and comparison of the arrival times and duration for each depth between the observed and synthetic waveforms. Features that we were looking for were similarities between the observed and synthetic waveforms, including duration, arrival times, and amplitude. By using this method, we were able to constrain a small range of depths for an event.

C. Results

Waveform inversion using source-side models with 3.0, 3.5, and 4.0 km water layers. Local water thickness determined which model would be used to make the synthetics. P-wave depth estimation was done for 14 outer rise earthquakes. 4 of those 14 events were in the Colombia outer rise and 10 were located in the Chile outer rise. For the Colombian earthquakes, the 3.5 km water layer velocity model gave the best fit and for the most of the Chilean earthquakes the 4.0 km water layer velocity model gave the best fit. The Chilean events of 03/03/01 and 04/09/01 had the best fits with the 3.5 km and 4.0 km water layer models,

respectively. It should be noted that the difference in fit of different water layer velocity models was small when the difference of water thickness was on the order of 0.5 km. To demonstrate that including the water layer resulted in a better fit, Figure 4.2 depicts the results of when the waveform inversion was run with a source-side model with 0.0 km water layer (that still includes the 0.64 km sediment layer) and 4.0 km water layer of the 04/09/01 event. The best fit values of the 0 km and 4.0 km water layer were 0.0924 and 0.3322 respectively.

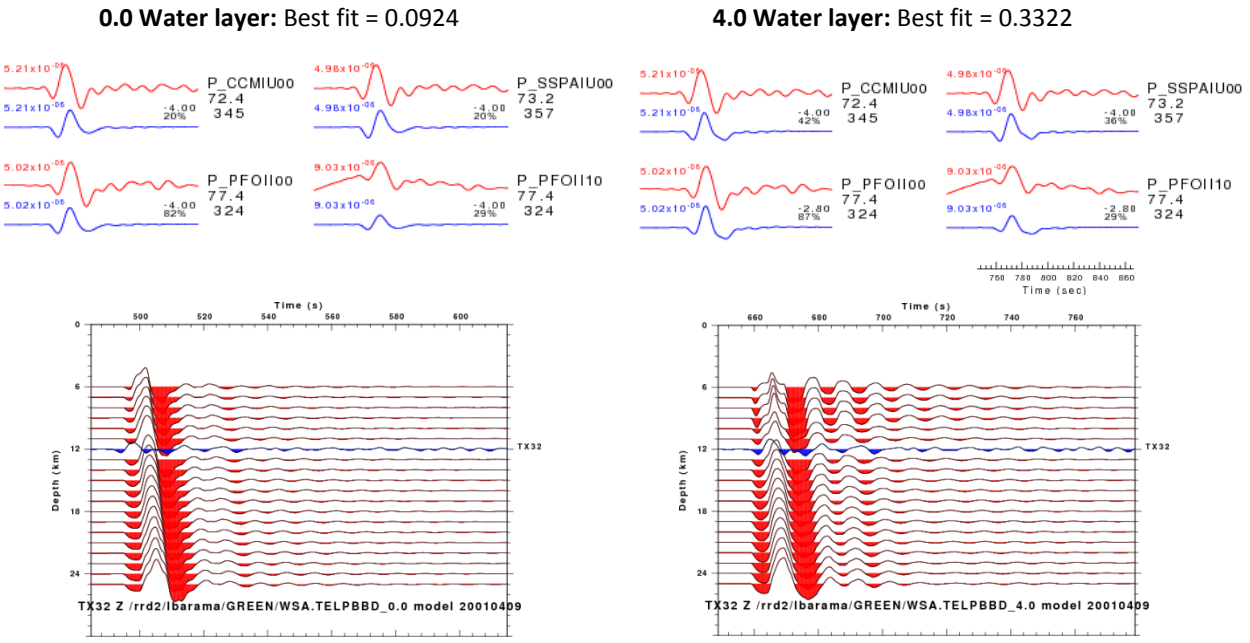

Figure 4.2. Comparison of waveforms for waveform inversion run with a 0.0 km water layer (top left) and a 4.0 km water layer (top right). The lower black number gives the percentage of variance reduction to characterize the individual goodness of fit. Comparison of waveforms in the P-wave depth estimation with a 0.0 km water layer (bottom left) and a 4.0 km water layer (bottom right). Note how the reverberations following the P-wave are related to the thickness of the water layer, with significantly more reverberations in the 4.0 water layer model.

The 10/21/10, $M_w = 5.93$ (GCMT) outer rise earthquake offshore central Chile is the event used in Figures 4.3 and 4.4. As shown in Figure 4.3a, this earthquake was recorded by 19 stations around the world. These stations are concentrated primarily to the north and south of the earthquake, with a single station in the east and no stations in the west. For the best fitting depth, Figure 4.3c-e shows the output of the waveform inversion, where each observed and predicted component is plotted to the same scale and peak amplitudes. The lower black number gives the percentage of variance reduction to characterize the individual goodness of fit, where 100% represents perfect fit [*Herrmann*, 2013]. The best fit for this earthquake was found to be 0.4391 at 9.0 km depth. The misfit function shown in Figure 4.3 b is peaked at the best depth but is relatively flat with depth change, as the fit slowly gets smaller with depth. The corresponding magnitude to the best fit was $M_w = 5.9$ with a strike, dip and rake of 235, 70 and -55. The focal mechanisms change with depth (Figure 4.3b) from a normal faulting with some strike slip component at shallow depths to strike slip at deeper depths, > 18 km.

Since the misfit function is relatively flat, displaying the small difference in fit with depth, we wanted to check the depth calculation. Therefore we compared waveforms with good signal to noise ratios (observed and picked from Figure 4.3 c) with the synthetic waveforms for different source depths. The synthetics are computed with the focal mechanism and magnitude found in the previous step, of $M_w = 5.85$, strike, dip, and slip of 235, 70, -55, and duration of 3.1 s. For all depth estimations, stations with a varied distribution of azimuths were chosen when possible (Figure 4.4a). For this earthquake, we used stations TSUM, DUFKYT, and QSPA, distributed east, southwest and south of the event (Figure 4.4a). Duration and arrival times were the features that influenced depth estimations. By plotting the observed waveforms along with the synthetics, we were able to compare arrival times, durations and amplitudes and

observe the effect of the water layer on the waveforms. The synthetic and recorded waveforms are shown in Figure 4.4b - d, with the preferred depth of 11 km. For these three stations, even though the peak and trough amplitudes do not have a perfect match, the duration and arrival of the P-wave appear to support a depth of 11 $\pm$ 2 km for the earthquake (Figure 4.4b-d). The duration of the trough of the initial arrival and peak helped to constrain where the best depth would be. Additionally, the reverberations after the P-wave are more pronounced for deeper depths 12-14 km, having three distinct troughs. The shallower waveforms did not really have this feature. The shape of the peak, particularly in Figure 4.4c, constrains the earthquake to be no deeper than 14 km depth. Note that station TSUM had the best matching waveform.

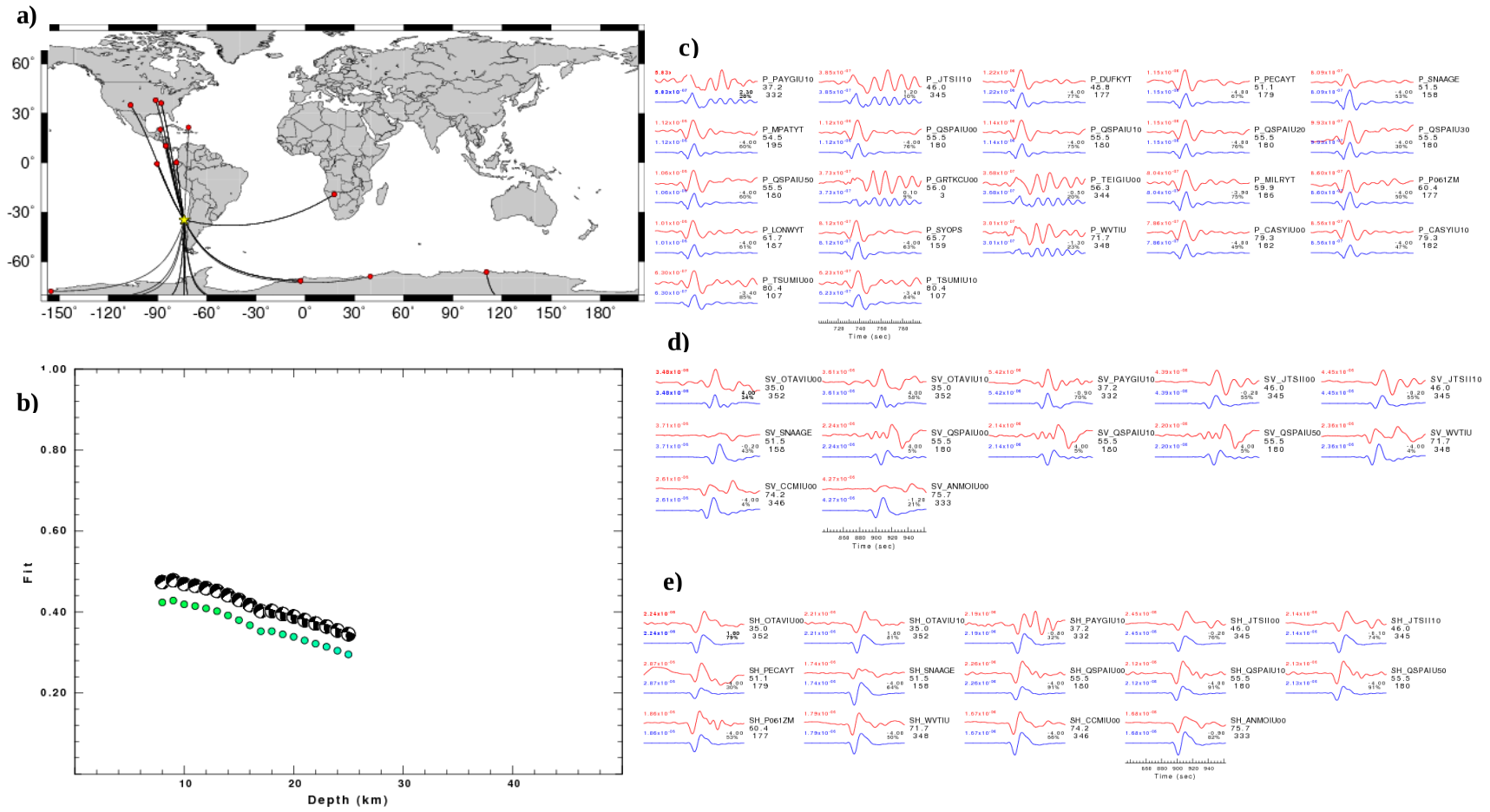

Figure 4.3. Waveform inversion results for the 10/21/2010 earthquake. (a) depicts a map of all stations used in the inversion with the yellow star as the epicenter and red dots are stations. (b) shows best fit as a function of depth with the best fit moment tensor and depth, strike, dip, slip, magnitude, and fit also displayed. P-, SH-, and SV- waves are shown in (c), (d), and (e), respectively. Plots for all other events are located in the Appendix. Traces are annotated with the time shift required for maximum correlation and the perent of variance reduction. Beneath the station name, the circle distance and source -to 0 receiver azimuth are given.

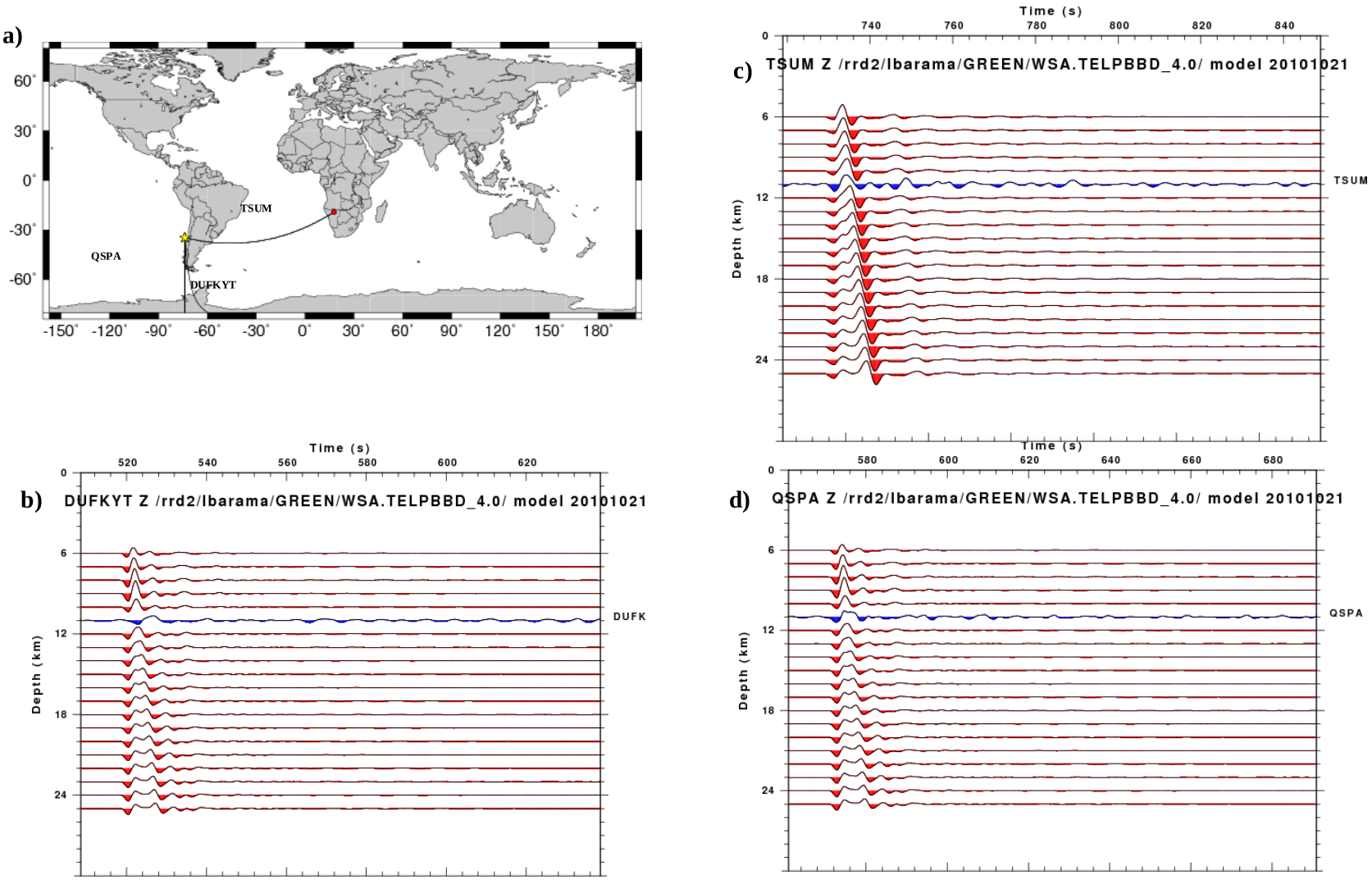

Figure 4.4. Depth Determination plots for the 10/21/2010 earthquake. **a)** shows the global map of stations used for the depth determination. The yellow star is the epicenter and the red dots are the stations. Figures (**b)-(d)** depict the observed seismogram in blue for the specific station and the synthetics in red. The x-axis shows time in seconds and the y-axis is depth in kilometers. The synthetic waveforms in these plots are the results of the wavefom inversion using the source-side velocity model with a water layer of 4.0 km. The waveforms of TSUM and QSPA support a depth of 11 km.

Table 4.3. Waveform inversion and focal depth estimation results, ordered from north to south, for all outer rise events in the Colombia and Chile regions. D denotes depth (km) from the surface (sea level). The bold event indicates the event that was previously studied.

			GCMT		Inversion Result						Depth Estimation
Date	**Lat(°)**	**Long(°)**	**D**	**M_w**	**D**	**M_w**	**Fit**	**Stk**	**Dip**	**Rake**	**~ D**
3 18 2007	4.7135	-78.4477	12.0	6.26	8.0	6.12	0.4700	33	42	-65	12 ±2
3 17 2007	4.6504	-78.4788	13.1	6.04	5.0	5.91	0.5003	58	39	-72	11 ±2
12 21 2002	3.8016	-78.9008	15.0	5.28	13.0	5.29	0.1828	24	77	-98	13 ±1
11 26 1994	2.8374	-79.5167	15.0	5.28	9.0	5.21	0.1224	163	68	-125	16 ±2
7 16 2006	-28.6865	-72.5420	12.0	6.22	19.0	6.20	0.2455	338	61	-13	19 ±2
4 9 2001	**-32.7825**	**-73.4024**	**15.0**	**6.68**	**10.0**	**6.83**	**0.3322**	**235**	**70**	**-75**	**12 ±1**
10 21 2010	-34.7048	-73.7885	12.0	5.93	9.0	5.85	0.4391	235	70	-55	11 ±2
6 28 2010	-37.7956	-75.1423	20.4	5.64	19.0	5.47	0.3526	105	85	-75	19 ±2
3 3 2001	-38.9114	-75.0435	15.0	5.87	19.0	5.74	0.0958	50	55	-120	18 ±3
4 1 1998	-40.3434	-75.0201	15.0	6.69	17.0	6.45	0.3992	255	55	-50	17 ±2
12 20 2000	-39.0725	-74.9239	15.0	6.46	9.0	6.25	0.3636	230	75	-55	15 ±2
11 12 2003	-39.9831	-74.9425	21.8	5.57	24.0	5.64	0.0885	204	73	115	24 ±1
11 22 2009	-39.6120	-74.9703	12.0	5.88	16.0	5.67	0.3336	275	81	-94	16 ±2
2 19 1996	-42.0793	-75.3099	15.0	5.99	23.0	5.68	0.1740	235	45	-55	18 ±1

Table 4.3 lists the results of the waveform inversion and depth estimation and the GCMT values for depth and magnitude. The depth ranges are from 5.0 – 24 km depth for the waveform inversion and 9 – 24 ±2 km depth for the P-wave depth estimation. From Table 4.3, earthquake depths appear to increase from north to south of the outer rise events, with the shallowest depths occurring in the Colombia region and the deepest depths occurring in Chile and more precisely south Chile. Figures from the waveform inversion and depth estimation for all 14 earthquakes are in the Appendix. The figures of the inversion include a station distribution map, fit vs. depth plot, and the synthetic and observed waveforms comparisons for P-, SH- and SV- waves. The figures for the depth estimation include map of station(s) used and plot(s) of the observed and synthetic waveforms for 5- 25 km source depths.

The earthquakes that occurred on 03/03/2001 and 11/12/2003 all have notably poor fits, 0.0958, and 0.0885 respectively. A good fit is on the order of 0.40 or larger. These small fits

can be attributed to poor quality waveforms with high signal-to-noise ratios. The 2/19/1996, 6/28/2010 and 11/12/2003 events among the deepest earthquakes at 23 km, 19 km, and 24 km depths respectively. 3/ 3/2001 and 11/12/2003 are also deep, at 19 and 23 km, but unreliable since waveforms did not have good signal to noise ratio and the fit is low (0.0958 and 0.0885 fits). The events with depth $\geq$ 19 km have reverse normal and thrust faulting mechanisms. Most of the shallower earthquakes have normal faulting focal mechanisms. The 2010 event is the most reliable deep earthquake, since it has the best fit of the deeper earthquakes (0.3526 fit). This event has a source depth of ~19km and shows thrust faulting characteristics from our calculated moment tensor from the waveform inversion.

The 04/09/2001, $M_w = 6.68$ (GCMT) outer rise earthquake offshore central Chile is the only event in this study previously studied. We found a focal depth of 10 km with $M_w = 6.83$ from the waveform inversion and 12 $\pm$1 km with the additional P-wave depth determination (Appendix). The *Fromm et al.* [2006] study found the depth of the 04/09/2001 earthquake to be no greater than 12 km depth, suggesting that rupture could possibly have occurred at depth of 10 to12 km with $M_w = 6.7$. The *Clouard et al.* [2007] study found a depth of 12 km but with $M_w = 7.0$. Similar to this study, both of these studies used teleseismic waveform inversion and waveform modeling to determine source depth and focal mechanisms. Additionally, these studies analyzed the aftershock sequence (through relocation) created by this earthquake. The range of depths of the aftershocks were from 16 to 46 $\pm$5 km [*Clouard et al.*, 2007]. Our estimated depths are similar to those of previous studies.

CHAPTER 5: DISCUSSION

Many studies have suggested that it is difficult to determine accurate hypocenter depths of shallow earthquakes occurring near deep sea trenches [e.g., *Yoshida et al.* 1992; *Lefeldt et al.*, 2009]. The teleseismic waveform inversion for earthquakes occurring in the study region suffers from a gap in the distribution of stations in the Pacific and Atlantic Oceans and perhaps the simplification of a 1-D Earth model. However, we were able to demonstrate that most events in this region are relatively shallow and have downdip normal mechanisms, typical of outer rise tensional earthquakes [*Lefeldt and Grevemeyer*, 2008]. The occurrence of shallow (~ 11- 12 km depth) events with $M_w \geq 5.5$ and the clustering of smaller magnitude outer rise earthquakes in the southern portion of Chile (32°S - 44°S, refer to Figure 2.2) leads us to infer that there is potential fluid penetration within the crust and mantle of the subducting Nazca plate in the Southern Chilean region. Furthermore, the shallower earthquakes in this study had more normal faulting focal mechanisms, whereas the deeper earthquakes have thrust, reverse normal, and strike slip characteristics. This difference is consistent with theories that the focal mechanism will change from normal faulting to thrust faulting as the rupture gets closer to the neutral plane [*Lefeldt and Grevemeyer*, 2008].

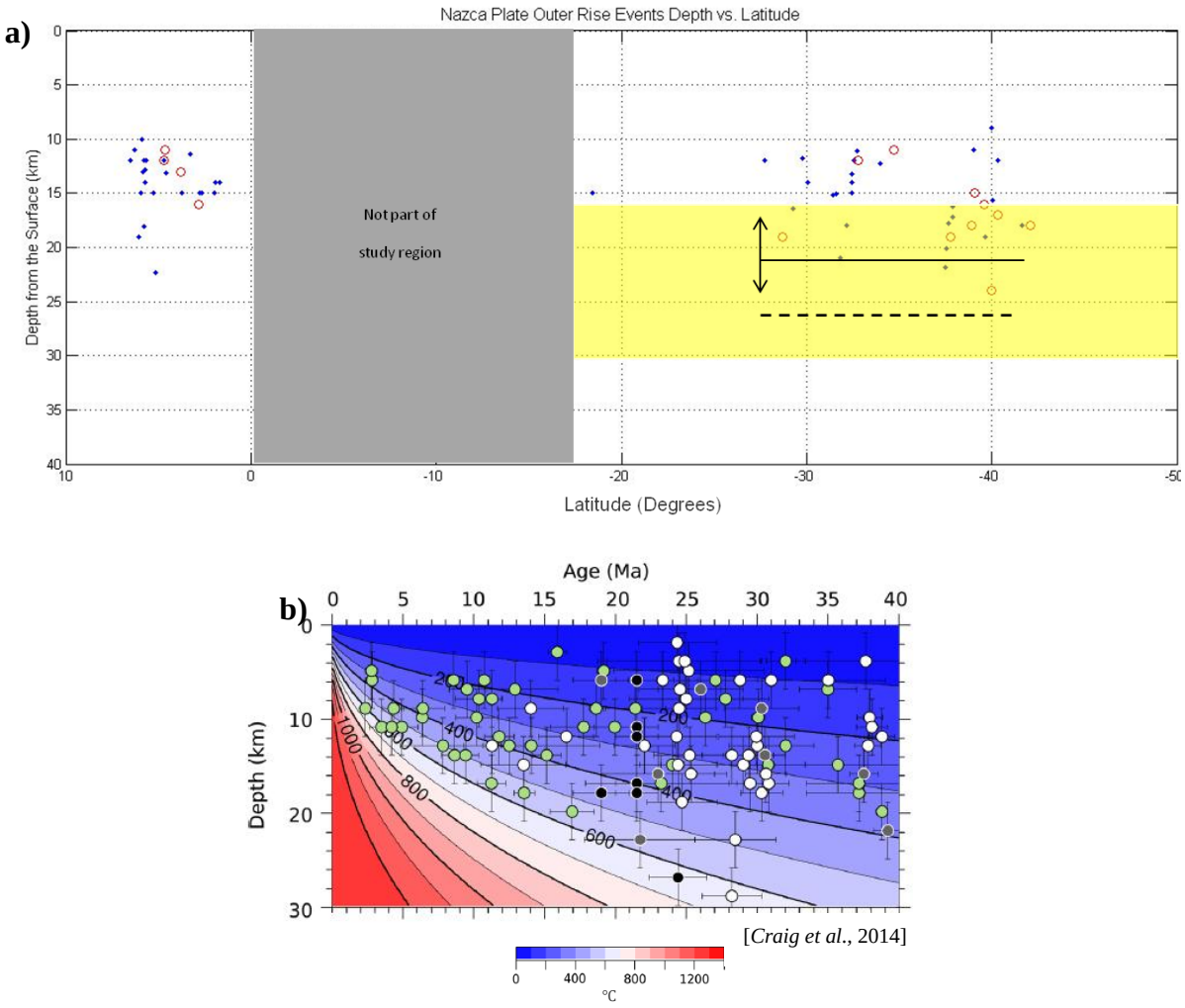

Figure 5.1 a) Depth vs. latitude plot of outer rise earthquakes used for waveform inversion in this study (red circles) and GCMT non-thrust faulting earthquakes within the vicinity of the outer rise $M_w \geq 5.0$ (blue points). The yellow box shows depth range where the 600℃ isotherm (neutral plane) was found to occur by *Craig et al.* [2014] The dotted and solid line with error bar represent the depths of the extent of brittle faulting (upper bound of neutral plane) approximated by the *Clouard et al.* [2007] and *Seno and* Yamanaka [1996] studies, respectively. **b)** Figure from *Craig et al.* [2014] earthquake depths plotted vs. plate age.

Figure 5.1a shows the distribution of outer rise earthquake focal depths with latitude. Earthquake depths plotted include those used in our study and additional events within the vicinity of the outer rise with $M_w \geq 5.0$ GCMT. Our depth estimates (shown in Figure 5.1a) are shallower than those of the Marianas outer rise and the global average studies of outer rise

events [*Chapple and Forsyth,* 1979; *Emry et al.,* 2014; *Craig et al.*, 2014]. The lithosphere in Colombia and Chile is younger and most likely thinner than the average subducting oceanic plate. Thus the global average depth of the neutral plane of 30-40 km found by the *Chapple and Forsyth* [1979] study is too deep for this region. Note that this region's seismicity and neutral plane are expected to be much shallower than the *Emry et al.* [2014] study in the Marianas. Therefore shallow depths and a shallower neutral plane than previous studies have approximated is plausible. In the Chile region, *Clouard et al.* [2007] suggest that tensional stress reaches the yield stress envelope at a depth of 22 km, asserting that brittle failure can occur up to 22 km depth with a neutral plane at 26 km depth (beneath the seafloor). Additionally, *Seno and Yamanaka* [1996] estimated a depth of 21 $\pm$4 km for the 450°C isotherm and neutral plane in Chile. From Figure 5.1a,we observe that the extent of earthquake depths found in this study (red circles) appears to correlate well with the *Clouard et al.*'s [2007] neutral plane of 26 km depth, and the 21$\pm$4 km neutral plane depth of the *Seno and Yamanaka* [1996] studies in Chile.

The yellow box in Figure 5.1a indicates the depth range over which the 600°C isotherm is expected to occur for Chile from the *Craig et al.* [2014] study based on the plate age [Muller *et al.* 2008] and the thermal models of McKenzie *et al.* [2005]. This isotherm extends to 16 - 35 km depth for Chile and shows the depth beneath which brittle failure should no longer occur. Neither this nor any study has yet to constrain the extent of brittle faulting or the neutral plane in the Colombian outer rise.

Knowing that the age of the Nazca plate ranges from approximately 6 - 40 Ma, Figure 5.1b shows that the ranges of depth for our study region corresponds to the *Craig et al.* [2014] thermal model of age and depth. The *Craig et al.* [2014] figure included in Figure 5.1b is a useful comparison for crust age, depth, and temperature. Recalling that the northern portion of

the Nazca plate 0° - 7°N is younger than the southern portions of the plate 20°S - 35°S [*Gutscher et al.,* 2000], the relatively shallower depths of earthquakes offshore Colombia compared to the Chile region seem to reflect the age difference and consequential lithospheric differences in temperature, thickness and rigidity. This suggests that temperature and age help define how deep brittle failure can go. The deeper depths of earthquakes also correspond to the region from 31°S - 41°S where the angle of subduction changes from shallower to steeper. We propose the primary constraints that define the neutral plane and the stress field are attributed to the bending of the lithosphere, with temperature as an additional constraint on the depth of brittle failure.

A model where the depth of the neutral plane varies both temporally and spatially was suggested by *Christensen and Ruff* [1983, 1988]. *Christensen and Ruff* [1988] found that tensional outer rise earthquakes tended to follow large underthrusting earthquakes, where the coupling between the subducting and overriding plate is weakened and thus tensional stresses from slab pull are transferred and accumulated in the outer rise. Compressional earthquakes in the outer rise are thus attributed to trench-perpendicular compression prior to a large thrust event [*Christensen and Ruff*, 1983, 1988]. *Lefeldt and Grevemeyer* [2008] plotted thrust events that occurred before the outer rise events in Middle America (down to 90 km depth) and used this to suggest that all the events in their study occurred after a partial decoupling of the incoming and the continental plate and thus are slab pull related. The neutral plane might change or occur deeper after the occurrence of large outer rise normal faulting events or before a large thrust event. In our study region, there are no large thrust events obviously related to or prior to large tensional outer rise events, and furthermore, this temporal and spatial relationship of the neutral plane is a simple cycle model, whereas the real world situations are much more complicated and non-linear.

The outer rise lithosphere is in a tensional state due to the effects of slab-pull [*Kanamori*, 1971]. Therefore the larger number of outer rise events in Chile than in Colombia could be due to the fact that the rate of convergence of the Nazca plate in Southern Chile is 8.0 - 8.4 cm/yr, thus producing more earthquakes than the Colombian region that has a convergence rate of ~6.0 cm/yr.

The 04/09/2001 event occurred in a region fractured by horst-and-graben type faults in between the O'Higgins seamounts and the Chile trench [*Clouard et al.*, 2007] and in close proximity to the Juan Fernandez Ridge. *Ranero et al.* [2005] found that bend related faults along the Juan Fernandez Ridge cut 15 - 20 km into the lithosphere and are most likely reactivated. They also suggest ridges that bend little at the trench will result in sparse shallow and deep seismicity and in little hydration. Perhaps this can be attributed to why there are so few outer rise events in northern Chile ~24°S, where the subduction dip angle is shallow and the crust is old (43-55 Ma) [*Gutscher et al.*, 2000].

However, the focal mechanism of the 04/09/2001 event was normal, shallow, and tensional which leads us to infer that it was the result of the nucleation of bending stresses, not the reactivation of faults correlated with the JFR or O'Higgins fault. Additionally, it should be noted that this event did not follow any large thrust event, as in the temporal and spatial cycle model of *Christensen and Ruff* [1988]. The compressional events of 10/16/1981 and 02/25/1982 are within the vicinity of the 04/09/2001 event, and those did precede the 1985 Valparaiso M_w= 8.0 earthquake which does seem to follow the ideal of some temporal relationship.

Only the past 20 years of earthquakes are useable in teleseismic waveform inversion, and furthermore, events in the outer rise with $M_w \geq 5.5$ do not occur frequently. The region offshore Colombia has the fewest outer rise events, as well as unique geology and outer rise seismicity

that has not been as extensively studied as the Chilean region. From Figure 5.1, we can infer that the extent of brittle failure is approximately 11 - 20 km depth offshore Colombia.

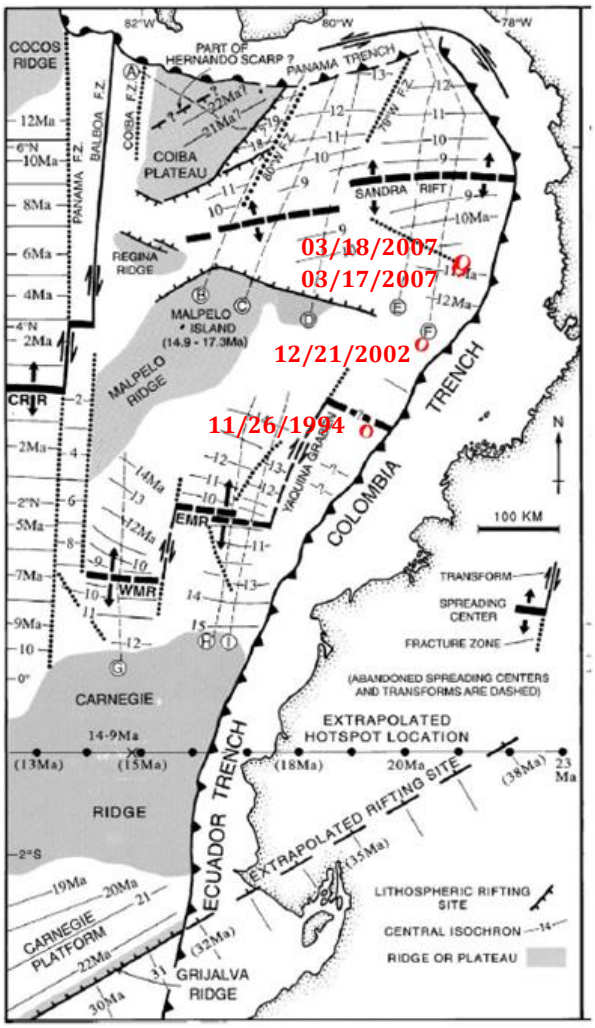

Figure 5.2 Plot of the Colombian outer rise earthquakes used in the waveform inversion, overlain on the *Lonsdale* [2005] interpretation of the geology of in the eastern Panama basin.

In Figure 5.2, the plot of the largest outer rise events used in waveform inversion for the Colombian outer rise is overlain on *Lonsdale's* [2005] map of the geology of the region. Figure 5.2 exemplifies the complexity of this region, and gives us insight into possible sources of earthquakes in the outer rise. From the plot, we observe that the earthquakes that occurred in the oldest portions of the plate in this region (~11 - 13 Ma) are near subducting faults, fracture zones

and rifts. The 03/17/2007 and 03/18/2007 are the northernmost events, and they appear to occur along a fracture zone oriented perpendicular with respect to the trench, south of the Sandra Rift. The 12/21/2002 event appears to be possibly influenced by the end of a long abandoned spreading center or transform oblique to the trench. The 11/26/1994 event occurred in close proximity to an unknown rift, no longer spreading [*Lonsdale*, 2005] north of the Yaquina graben. These observations lead us to infer that these outer rise events are not due to the reactivation of pre-existing faults due to subducting features in this region. These new faults must have been a result of the bending forces as the Nazca plate subducts since the focal mechanism orientations do not match the perpendicularly subducting pre-existing faults. Although the pre-existing faults could have weakened the plate already, and the earthquakes in this study may be the further rupture of the faults created by lithospheric bending stresses.

CHAPTER 6: CONCLUSIONS AND FUTURE WORK

Both the Colombia and Chile outer rise undergo far more extensional faulting than compressional faulting. There were no compressional events within the time frame of the data used in this study, which makes it difficult to constrain the neutral plane. The most recent compressional events in the Chile outer rise were the events of 1981 and 1982 at 30 and 27 km depth, respectively [*Clouard et al.*, 2007]. These depths of compressional events seem to correspond with our inference that the extent of brittle failure is at ~25 km depth for the Chile region. For Colombia, we infer that the extent of brittle faulting is ~15-20 km depth. We infer that these depths are possibly the extent to which water can penetrate into the lithosphere. Whether or not subducting features impact the nucleation of outer rise earthquakes is still not constrained but unlikely, since the gaps in outer rise event clusters along the Nazca plate still have subducting structures such as the Peru basin, Easter Fault zone and Nazca Ridge, and Chile basin within the vicinity of 12°S, 18°S, and 20°S – 30°S.

In future studies, we would like to incorporate the loading history of the plate to calculate the yield stress envelopes for the oceanic lithosphere in the outer rise. If tomographic data were available in the study areas, comparing our results with that of the extent of brittle failure to the depth of water logged faults would help constrain the depth of hydration and brittle failure. Additionally, we could investigate our method further by incorporating smaller magnitude outer rise earthquakes and the earthquakes occurring landward of the trench but still within the subducting Nazca plate. By expanding our methods thusly, we could further constrain the state of stress within the Nazca plate.

APPENDIX

Waveform Inversion results and Depth Estimation plots for all earthquakes.

All plots follow the following descriptions:

Waveform Inversion Plots: (**a**) Depicts a map of all stations used in the inversion with the yellow star as the epicenter and red dots as stations. (**b**) Shows best fit as a function of depth with the best fit moment tensor and depth, strike, dip, slip, magnitude, and fit also displayed. P-, SH-, and SV- waves are shown in c, d, and e respectively. The upper black number to the right of each predicted trace is the time shift required for maximum correlation between the observed and predicted traces. The lower black number gives the percentage of variance reduction to characterize the individual goodness of fit.

Depth Estimation Plots: (**a)** shows the global map of stations used for the depth estimation. The yellow star is the epicenter and the red dots are the stations. Figures b and onward depict the observed seismogram in blue for the specific station and the synthetics in red. The x-axis shows time in seconds and the y-axis is depth in kilometers.

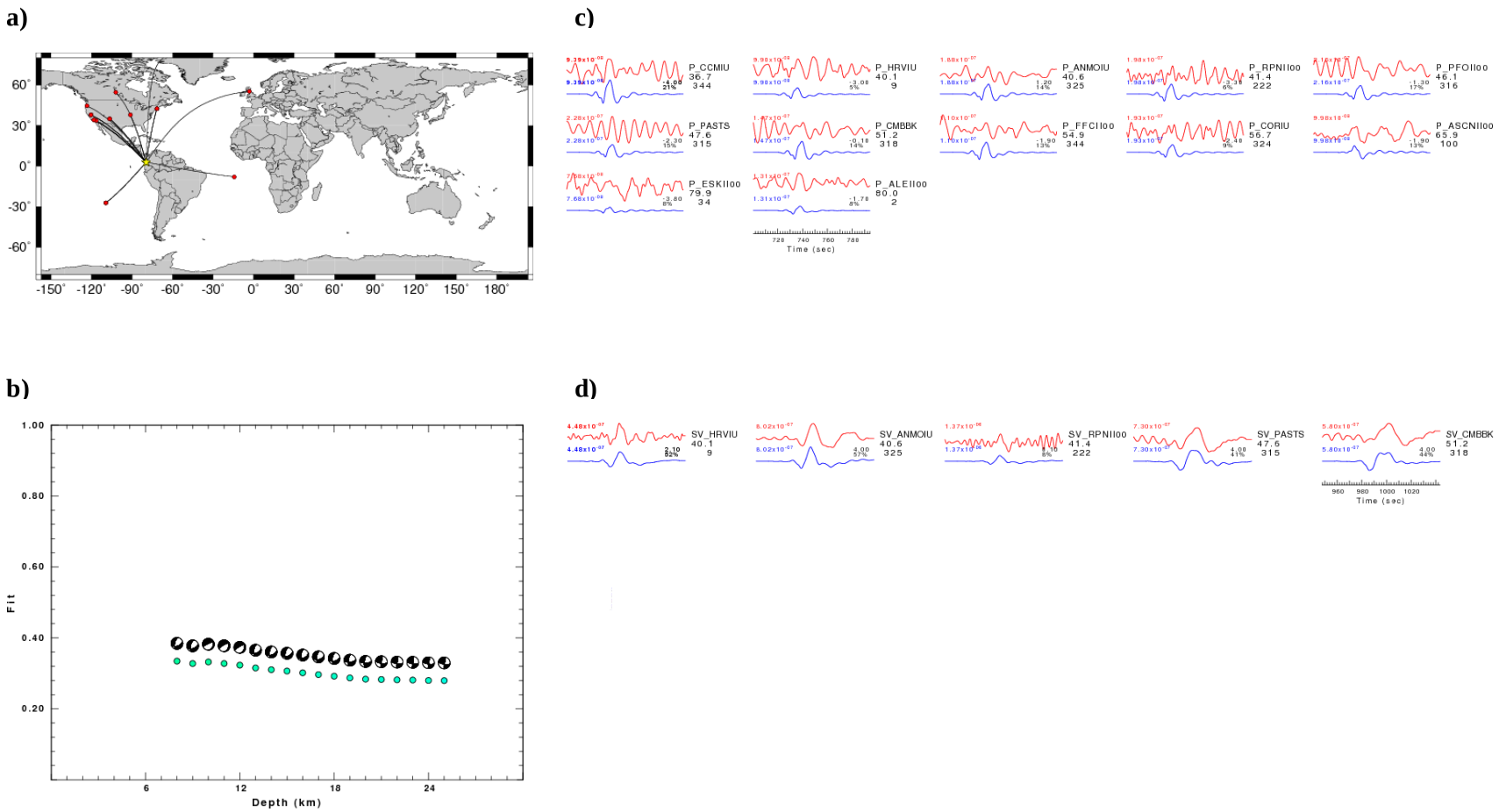

Figure A.1.1 Waveform inversion results for the 11/26/1994 earthquake. Refer to description of Figure 4.3.

a)

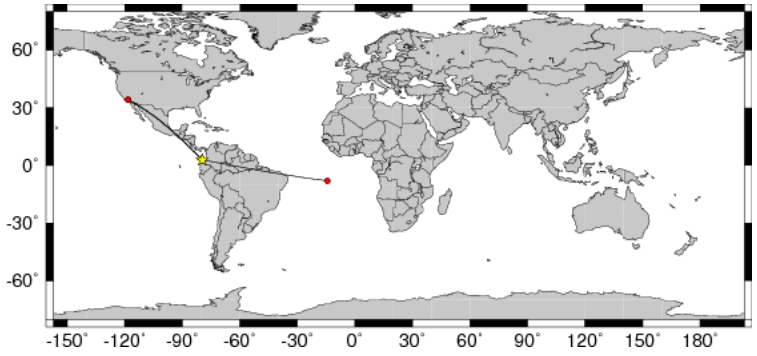

b)

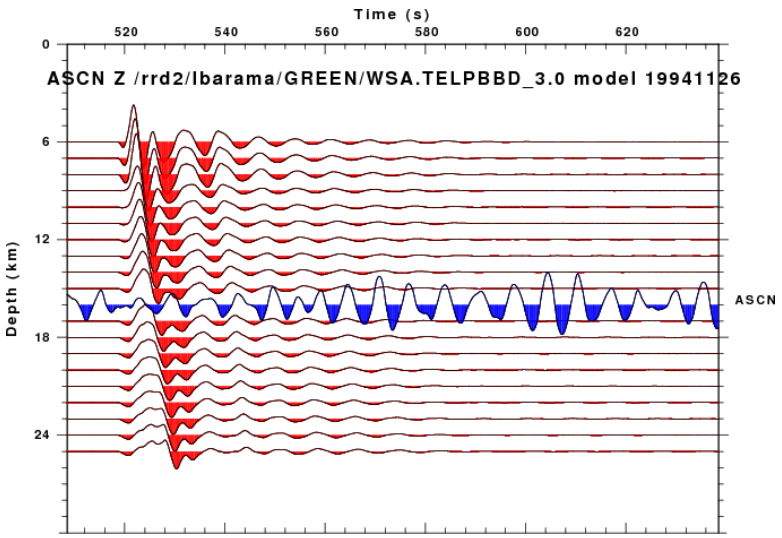

c)

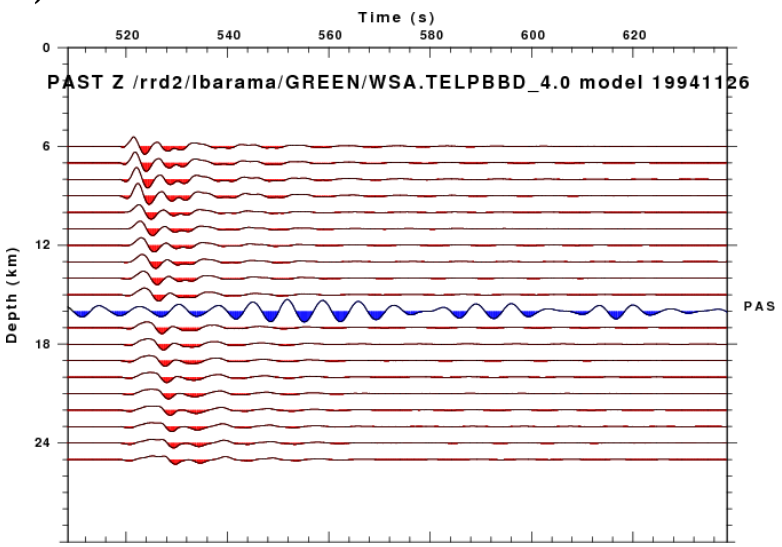

A.1.2Depth Estimation . Refer to description of Figure 4.4.plots.

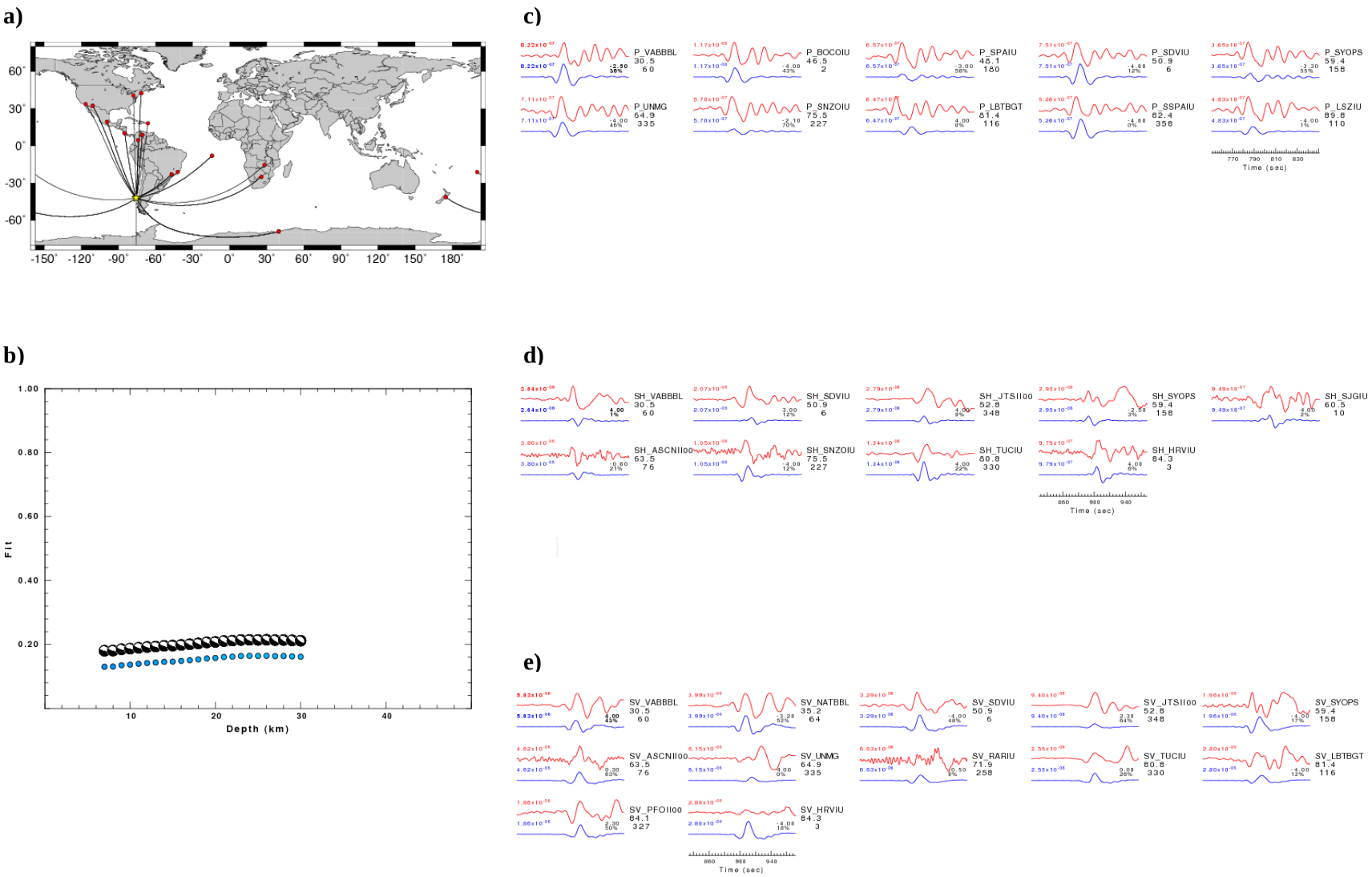

Figure A.2.1 Waveform inversion results for the 02/19/1996 earthquake. Refer to description of Figure 4.3.

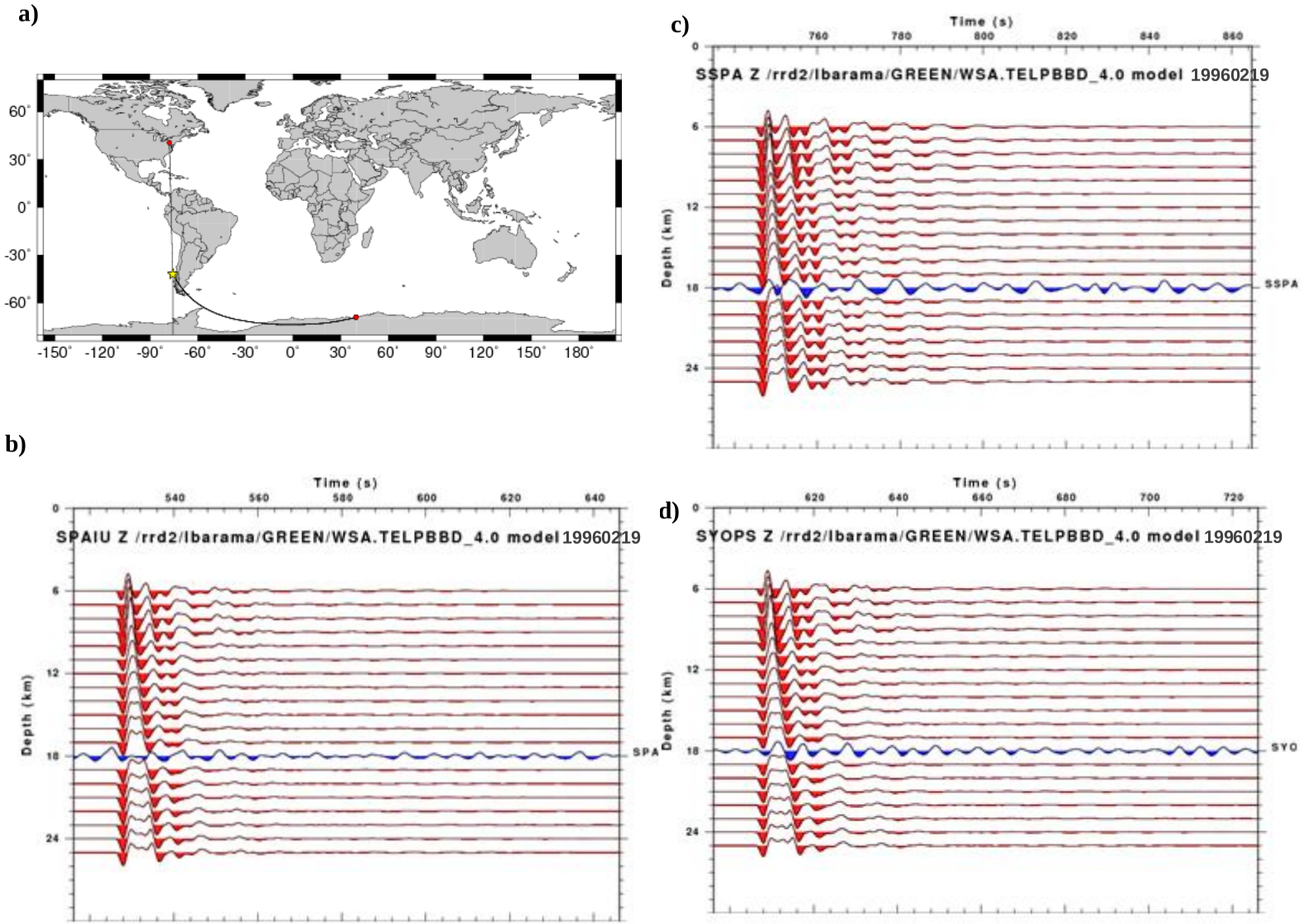

Figure A.2.2 Depth Estimation . Refer to description of Figure 4.4.

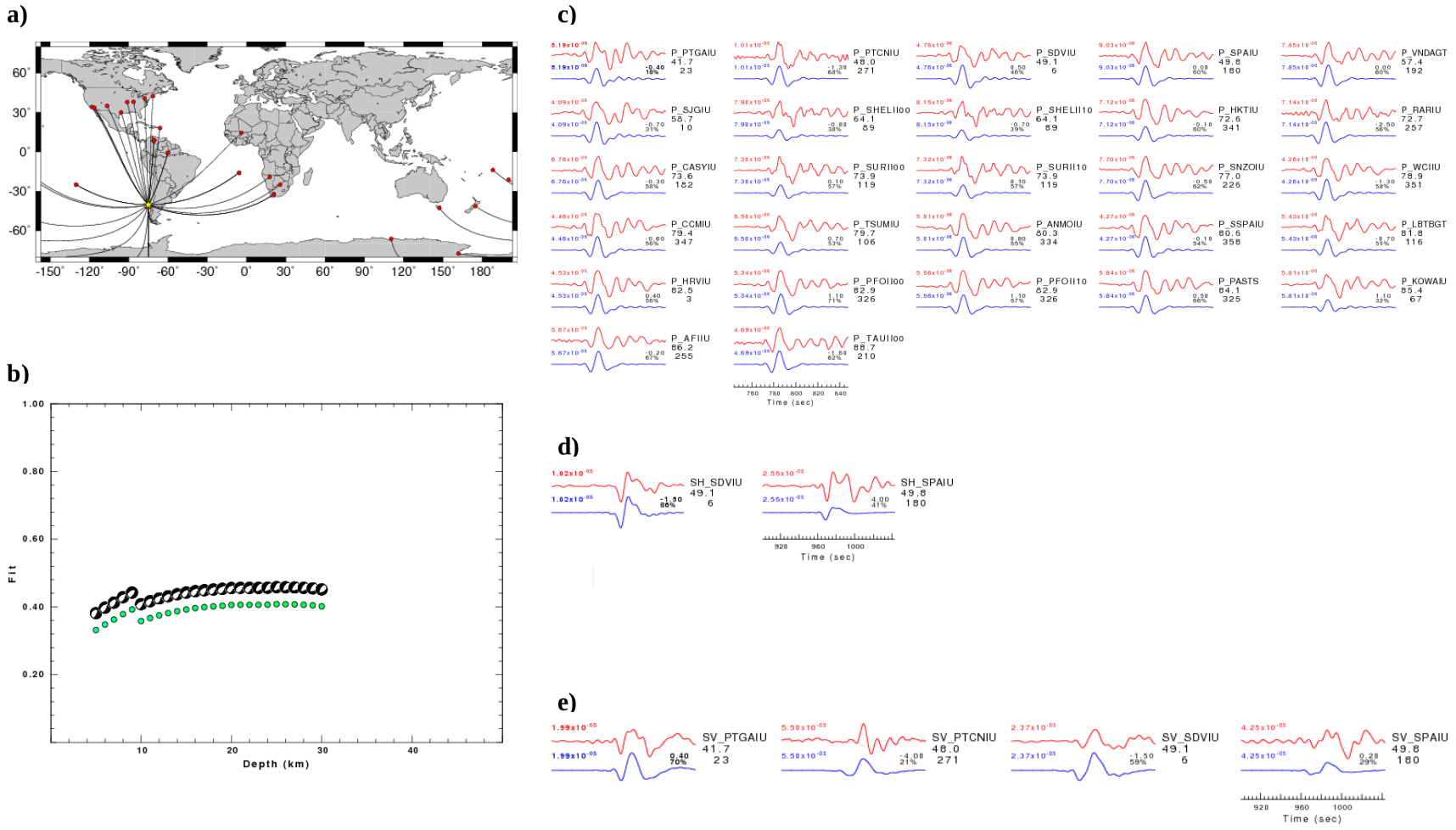

Figure A.3.1 Waveform inversion results for the 04/01/1998 earthquake. Refer to description of Figure 4.3.

a)

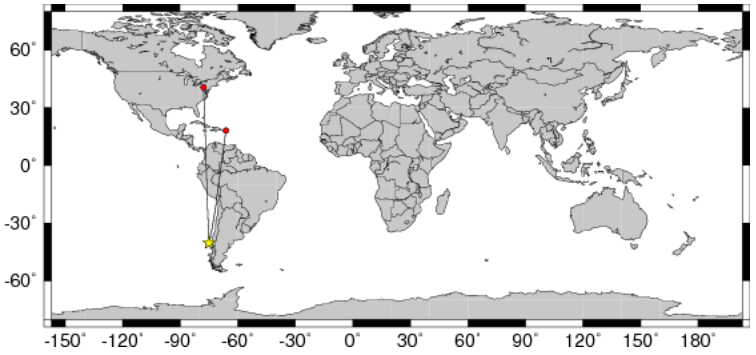

c)

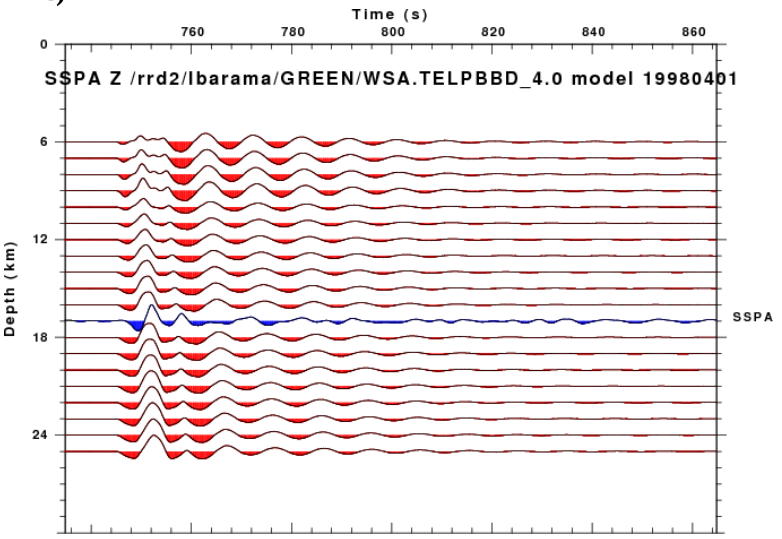

b)

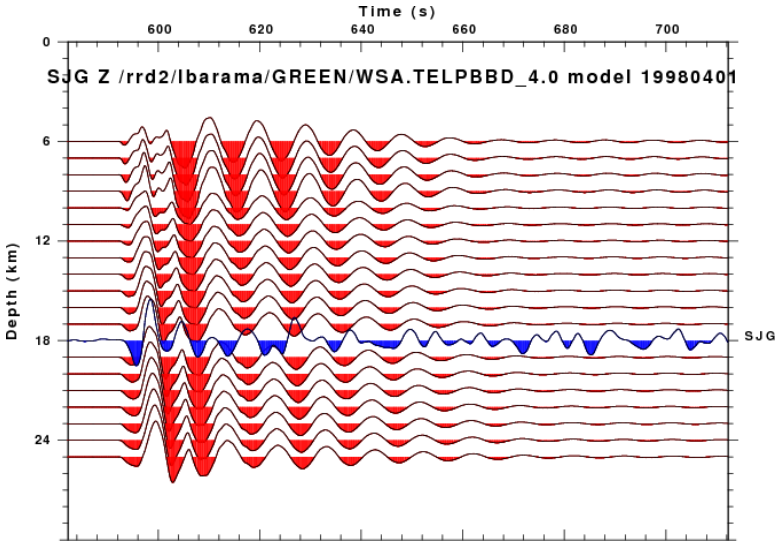

A.3.2 Depth Estimation . Refer to description of Figure 4.4.

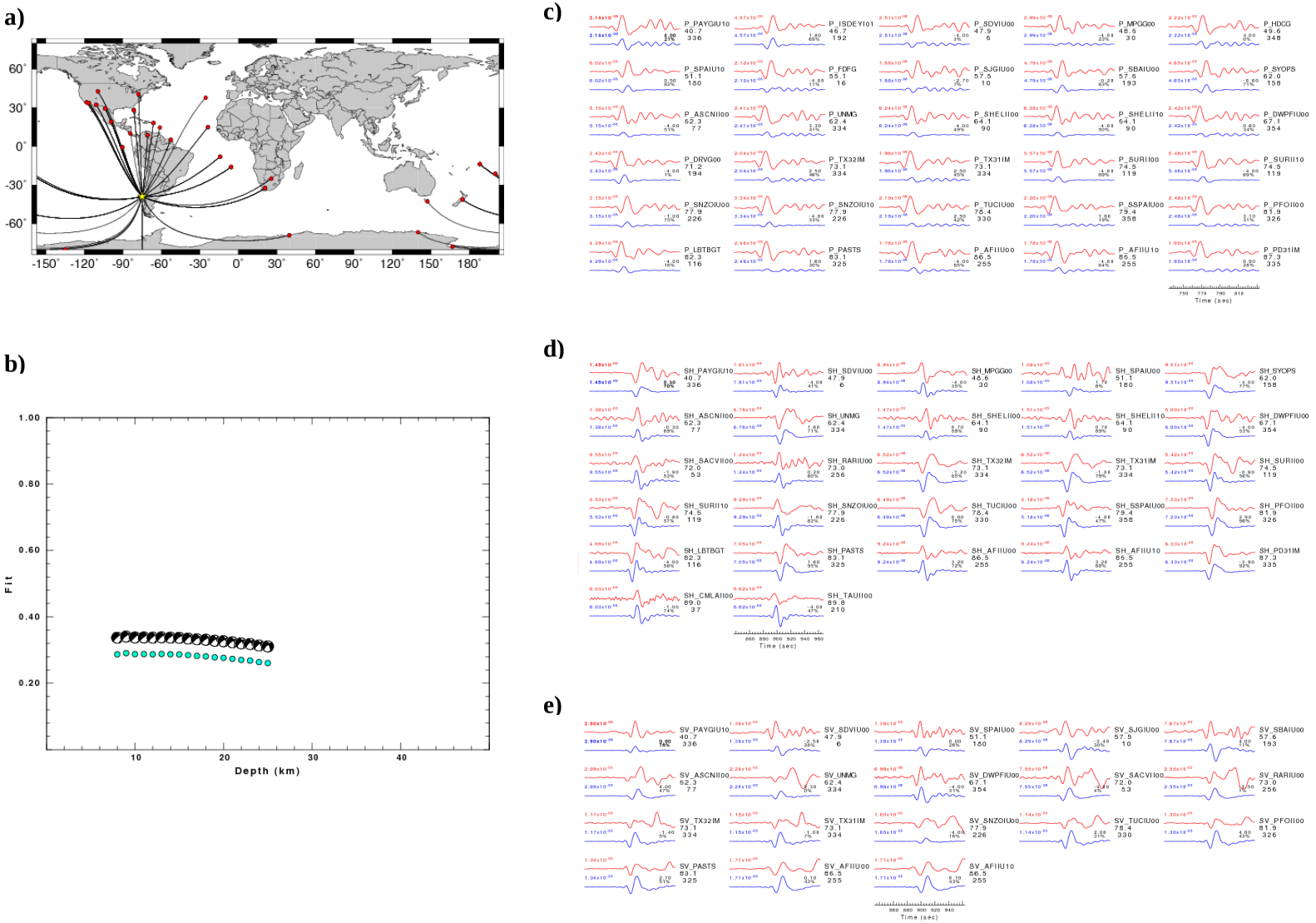

Figure A.4.1 Waveform inversion results for the 12/20/2000 earthquake. Refer to description of Figure 4.3.

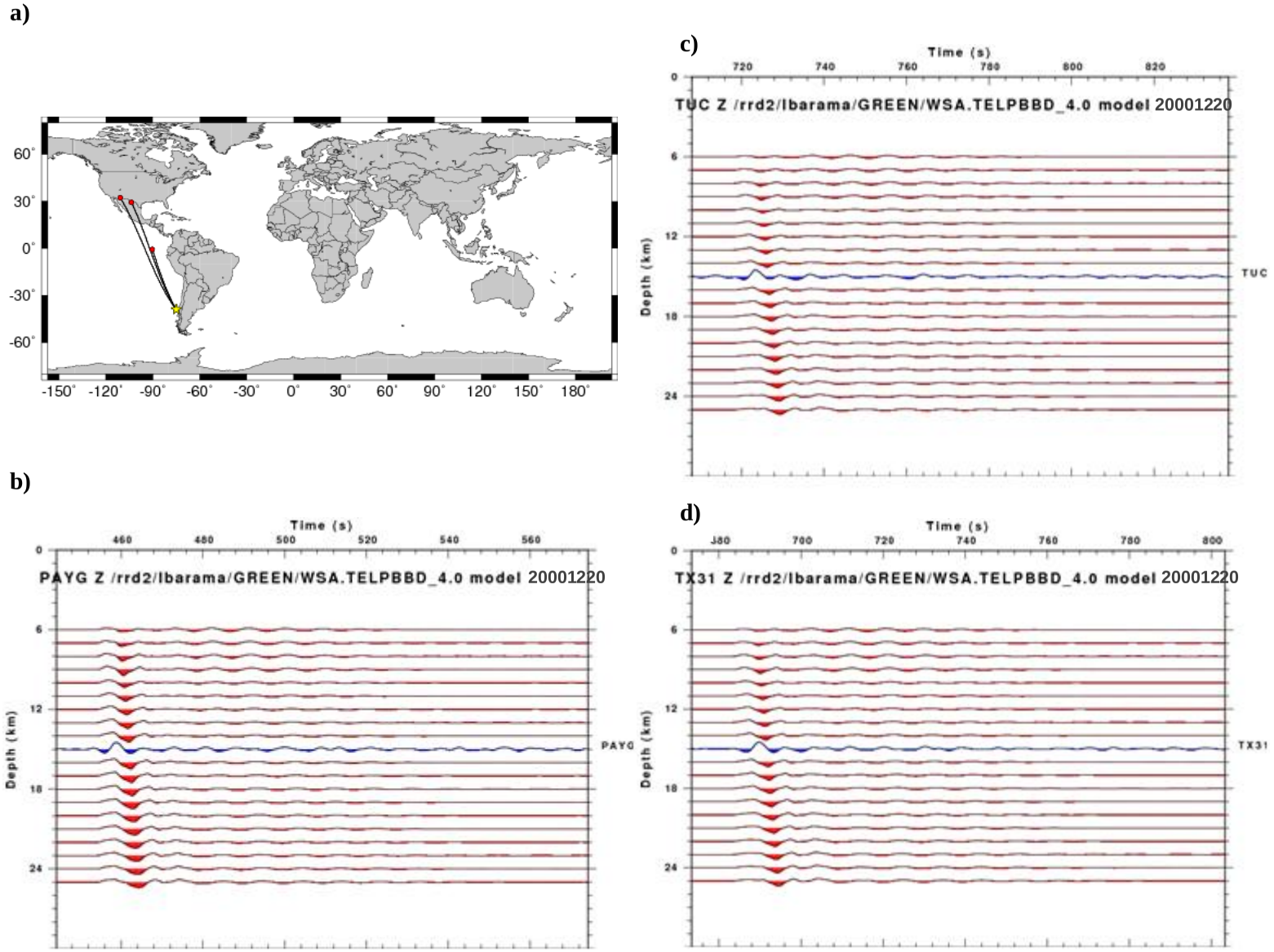

Figure A.4.2 Depth Estimation plots. Refer to description of Figure 4.4.

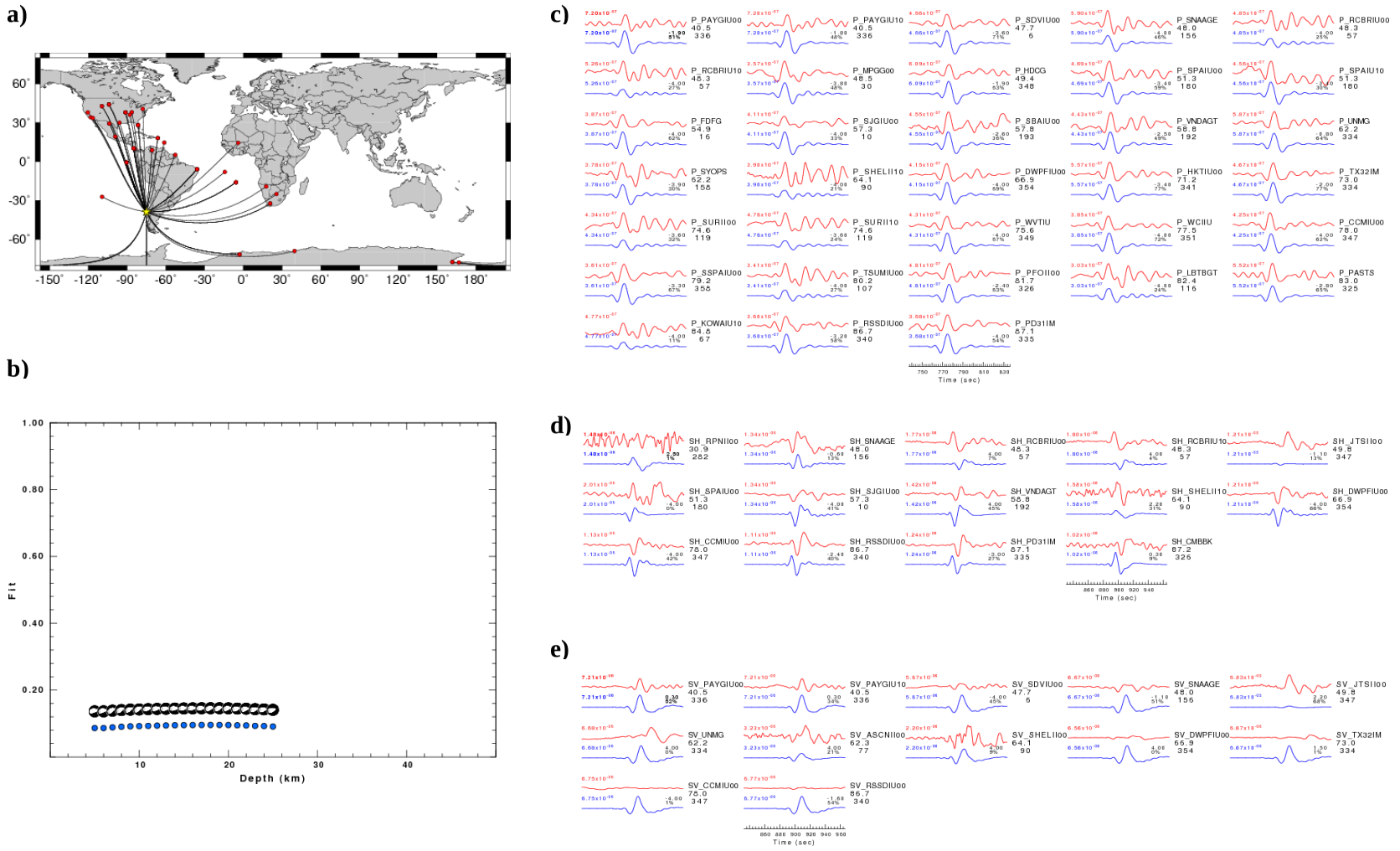

Figure A.5.1 Waveform inversion results for the 03/03/2001 earthquake. Refer to description of Figure 4.3.

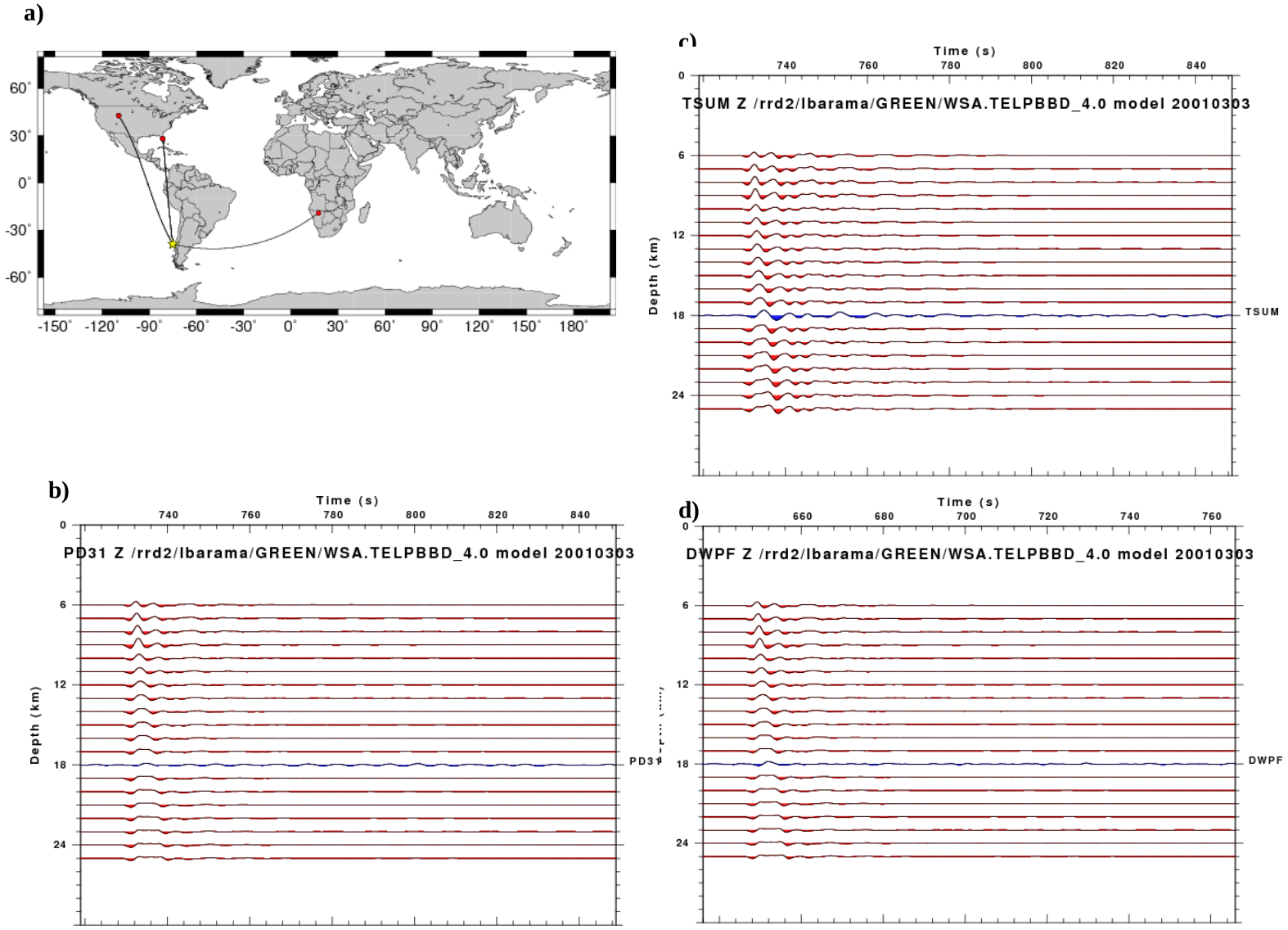

Figure A.5.2 Depth Estimation plots. Refer to description of Figure 4.4.

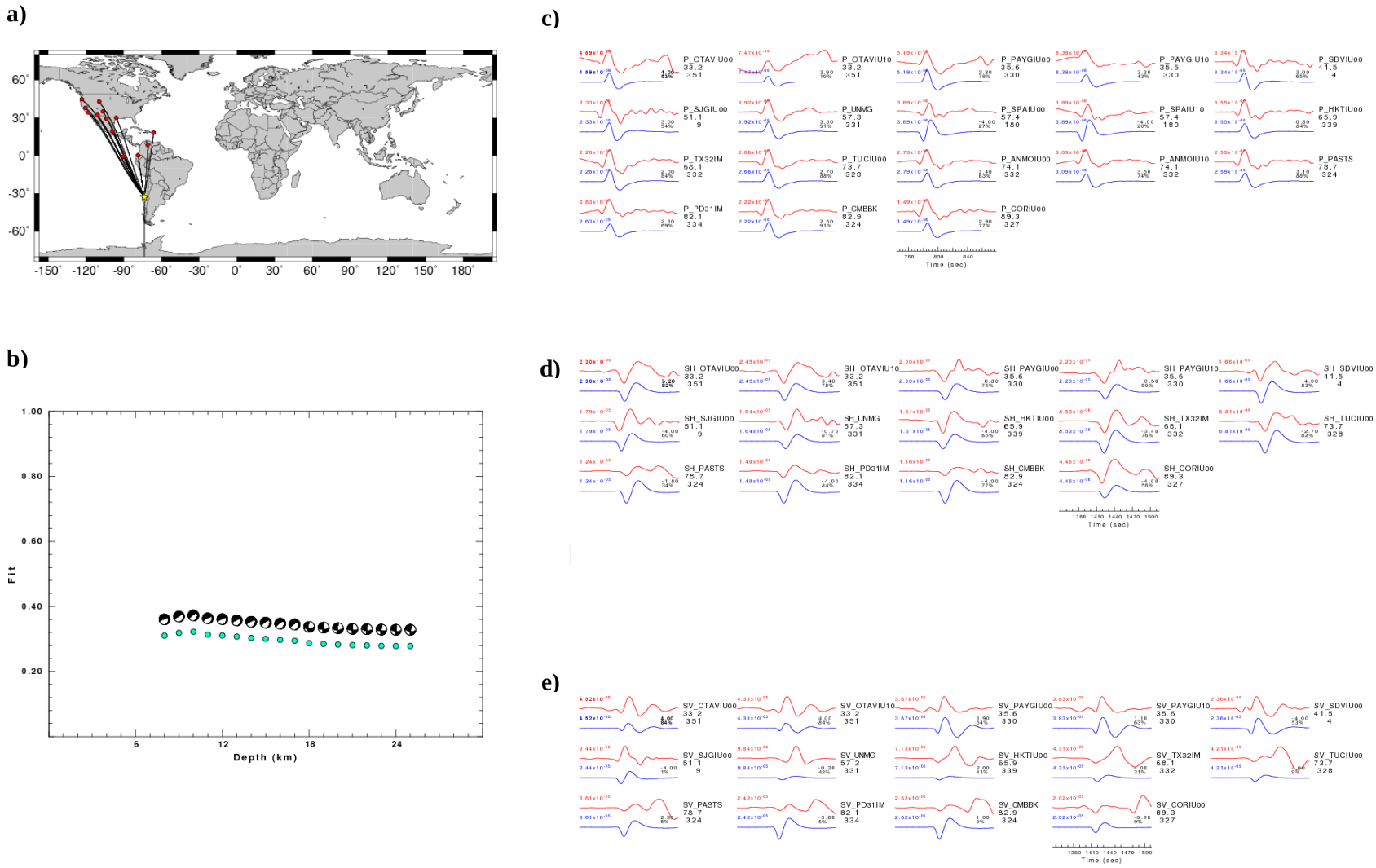

Figure A.6.1 Waveform inversion results for the 04/09/2001 earthquake. Refer to description of Figure 4.3.

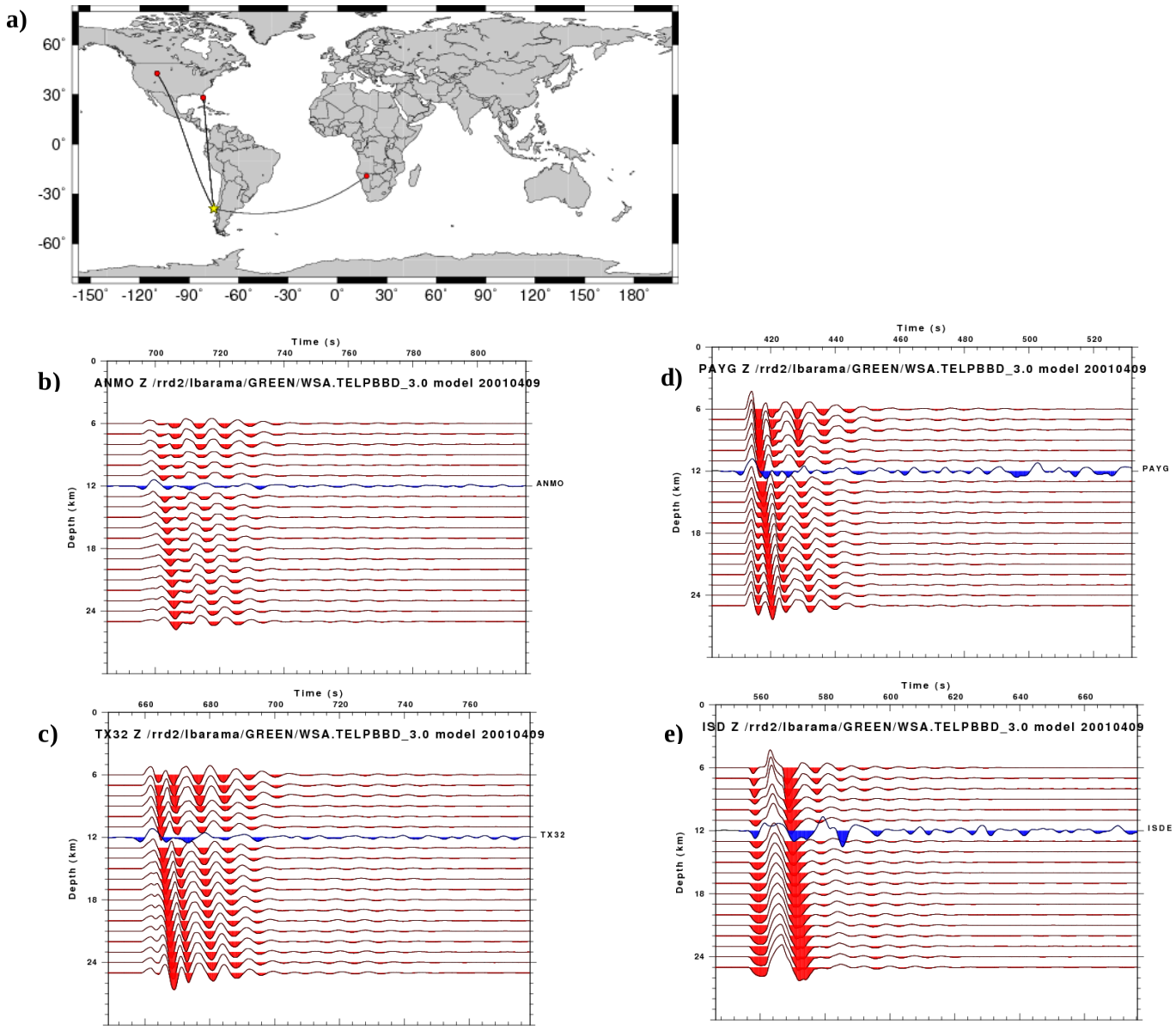

Figure A.6.2 Depth Estimation plots. Refer to description of Figure 4.4.

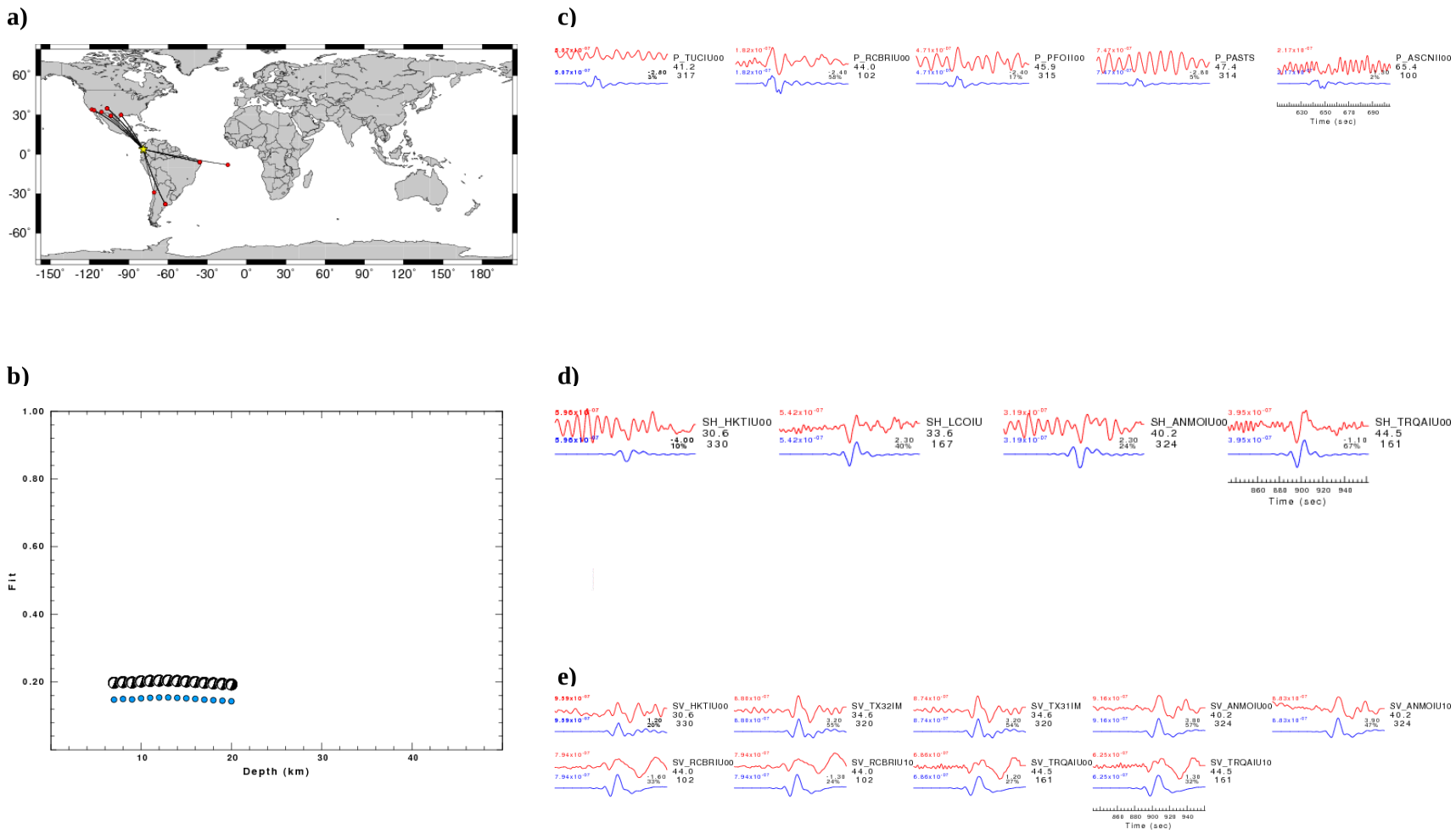

Figure A.7.1 Waveform inversion results for the 12/21/2002 earthquake. Refer to description of Figure 4.3.

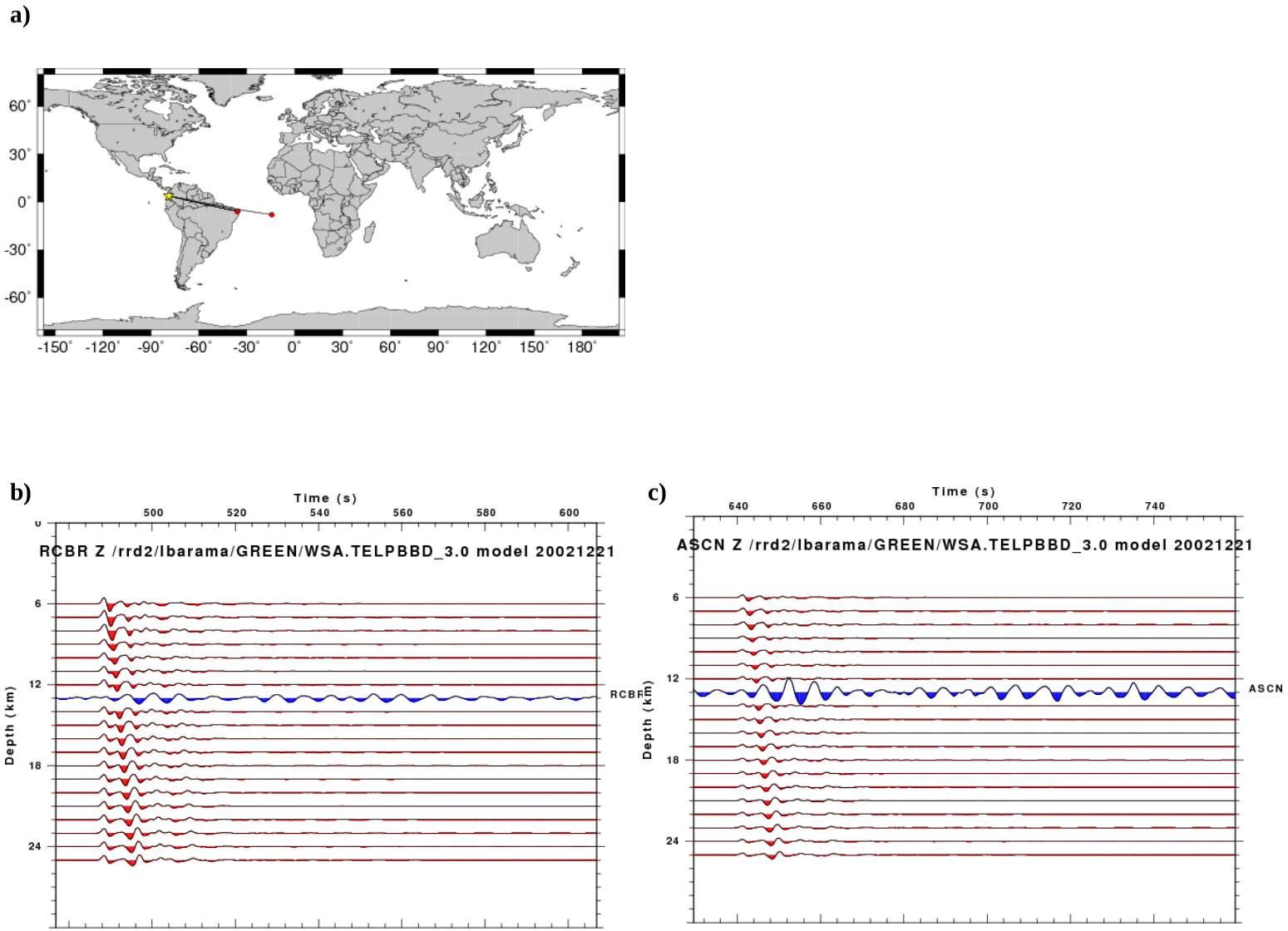

FigureA.7.2 Depth Estimation plots. Refer to description of Figure 4.4.

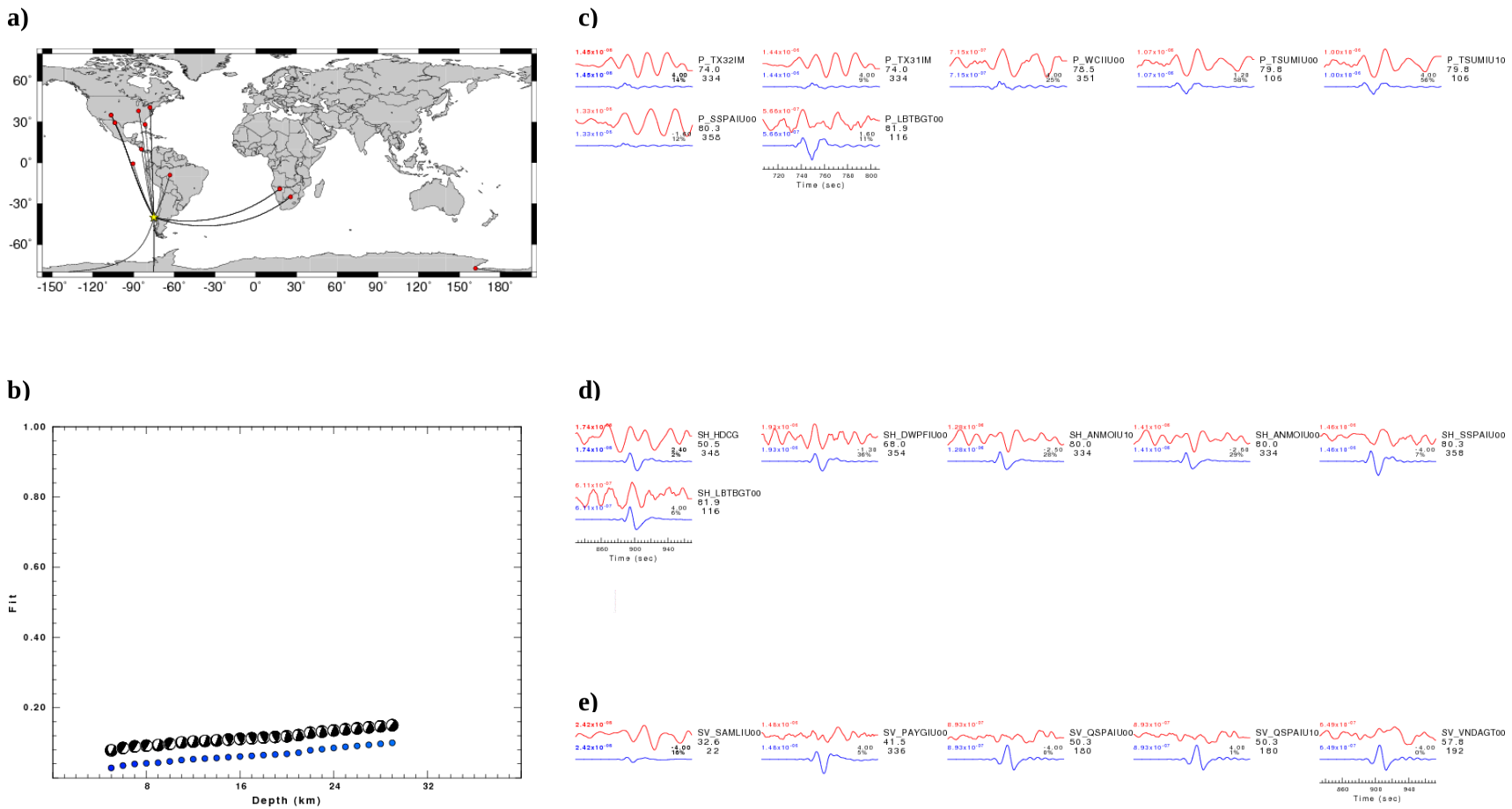

Figure A.8.1 Waveform inversion results for the 11/12/2003 earthquake. Refer to description of Figure 4.3.

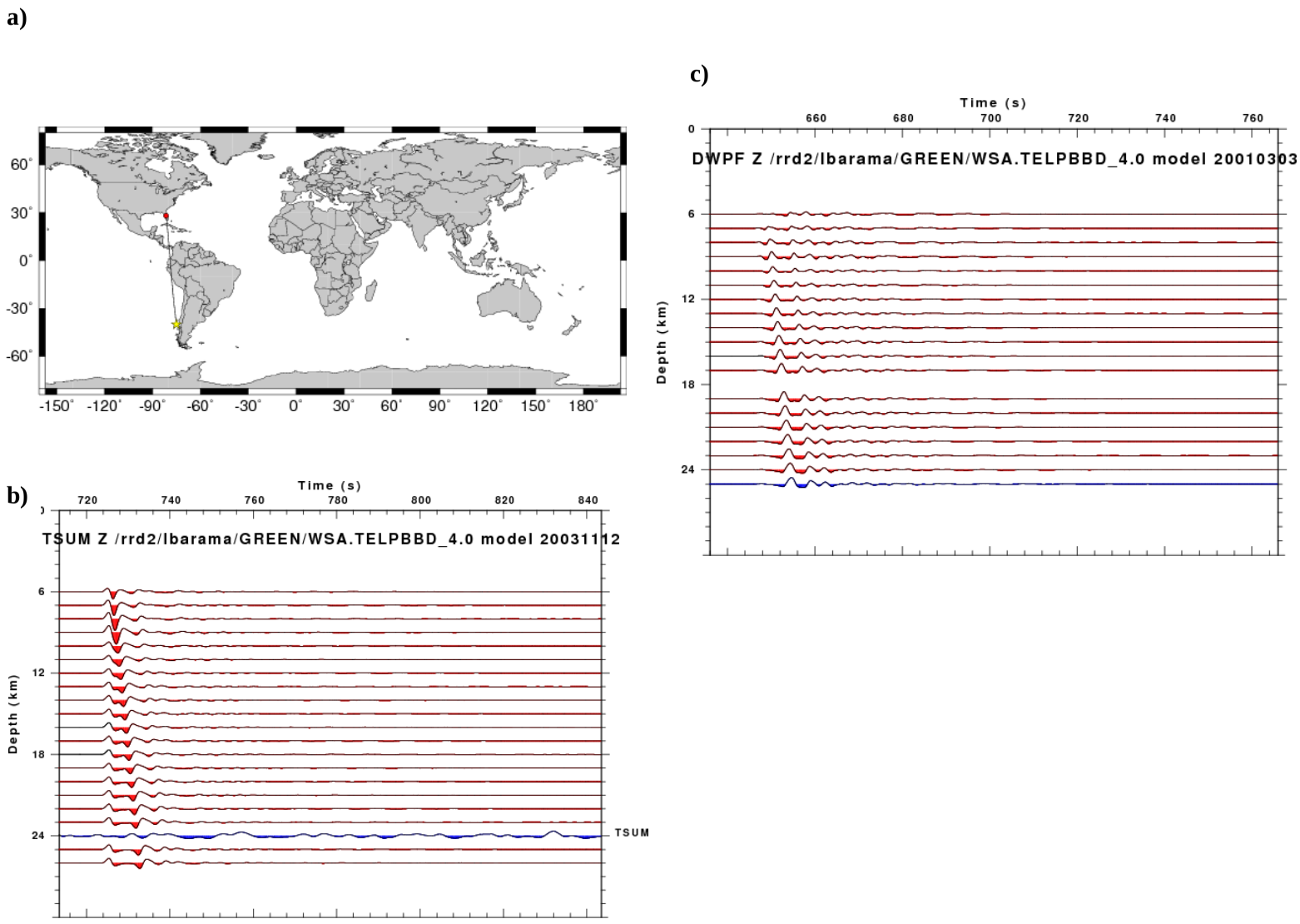

Figure A.8.2 Depth Estimation plots. Refer to description of Figure 4.4.

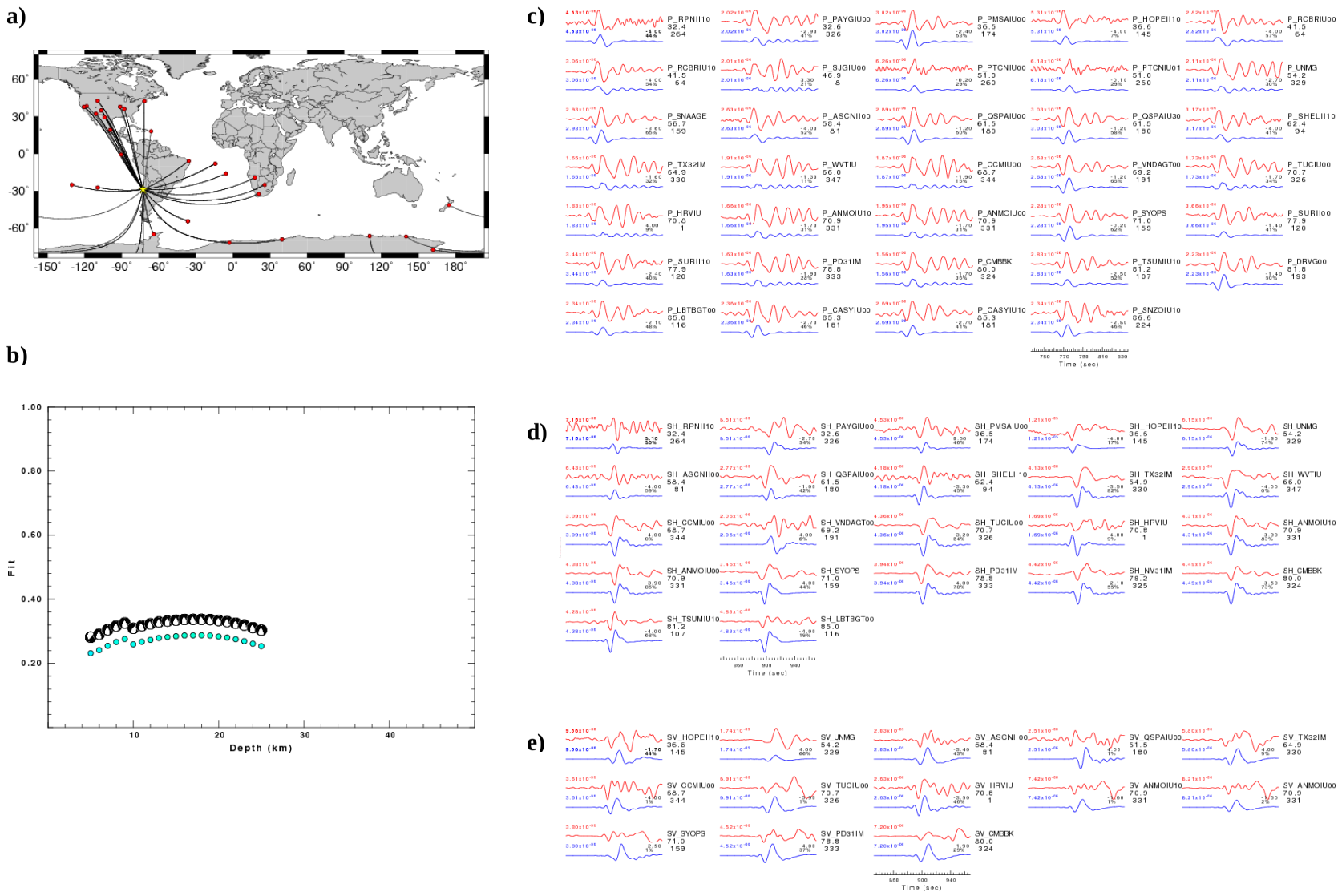

Figure A.9.1 Waveform inversion results for the 07/16/2006 earthquake. Refer to description of Figure 4.3.

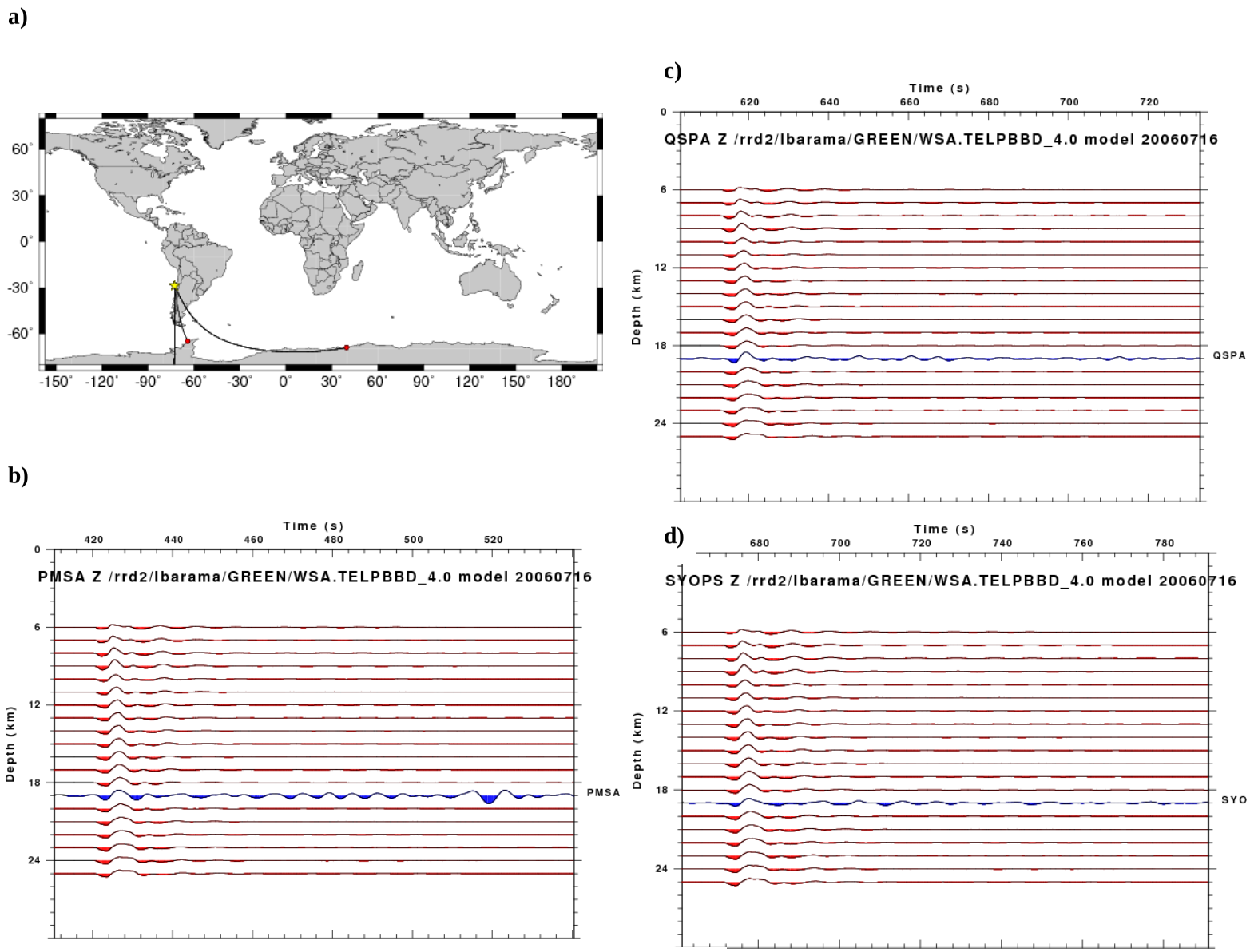

Figure A.9.2 Depth Estimation plots. Refer to description of Figure 4.4.

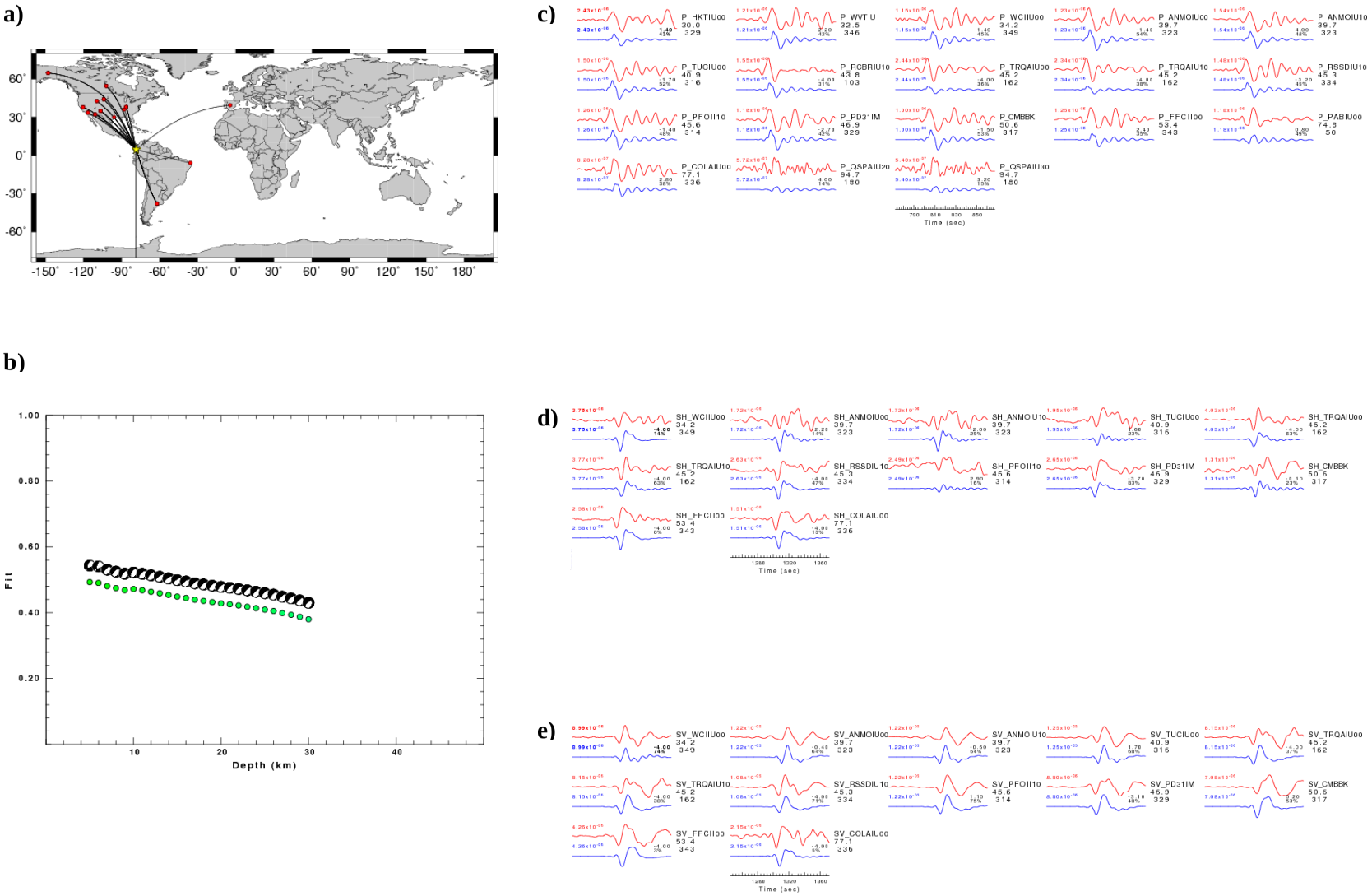

A.10.1 Waveform inversion results for the 03/17/2007 earthquake. Refer to description of Figure 4.3.

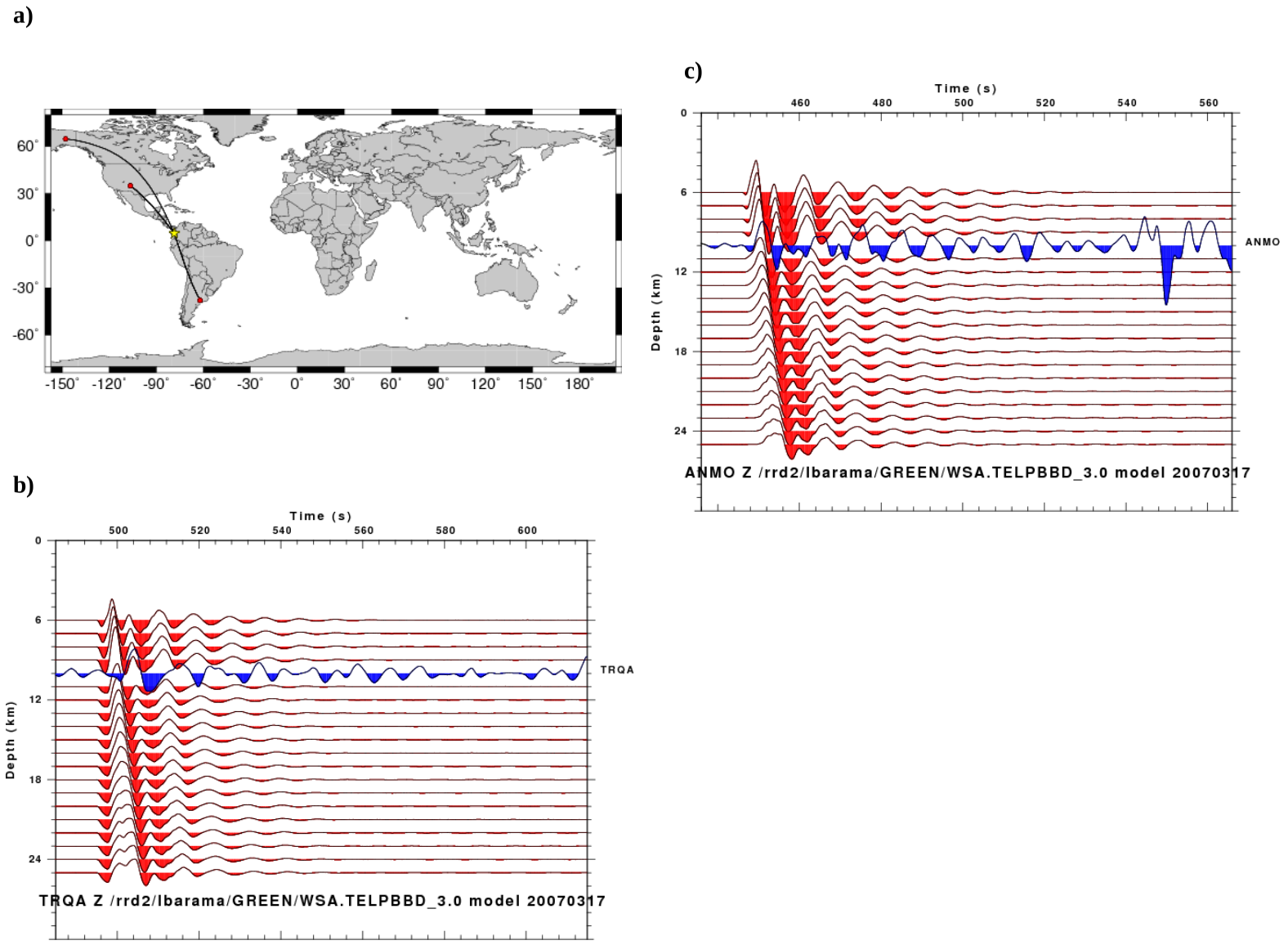

Figure A.10.2 Depth Estimation plots. Refer to description of Figure 4.4.

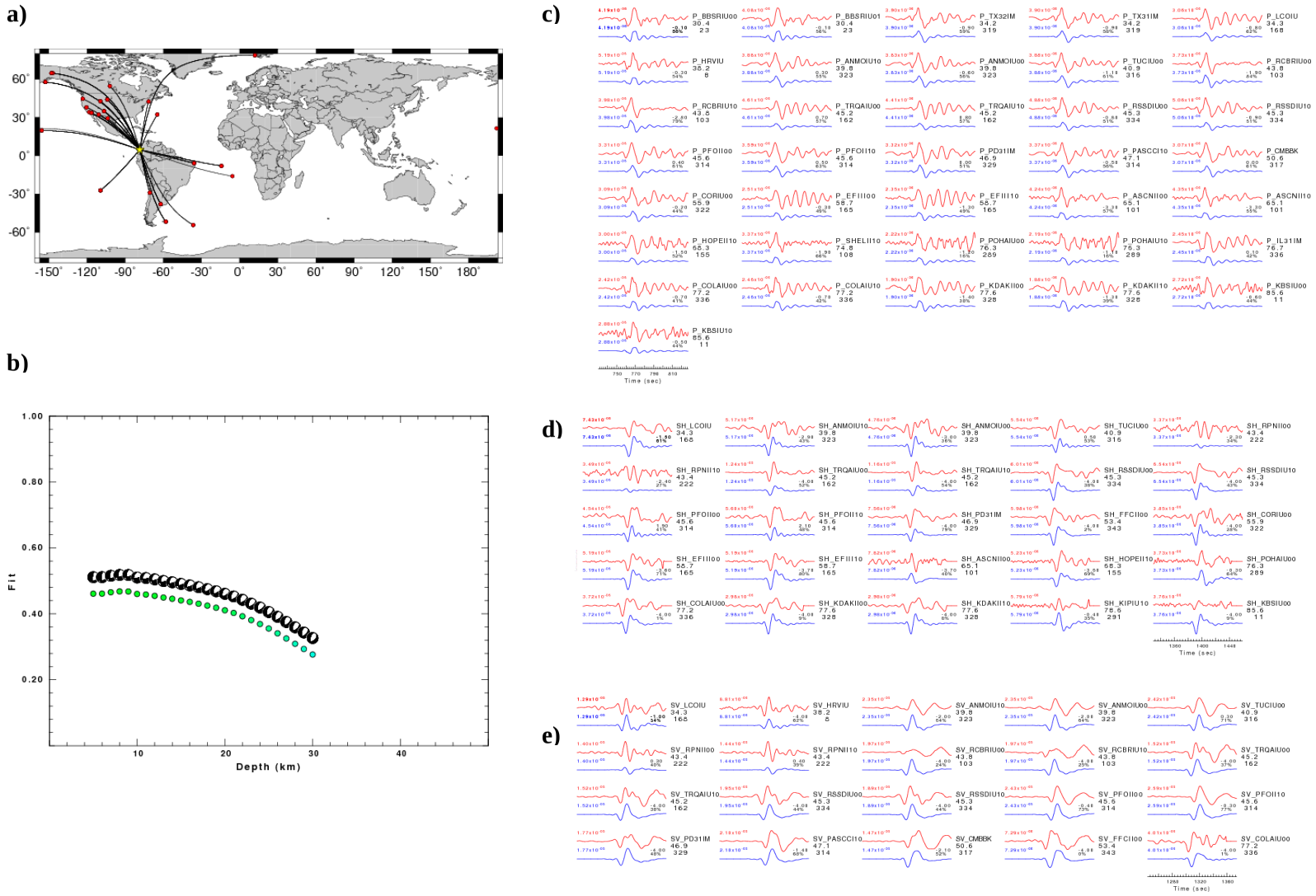

Figure A.11.1 Waveform inversion results for the 03/18/2007 earthquake. Refer to description of Figure 4.3.

a)

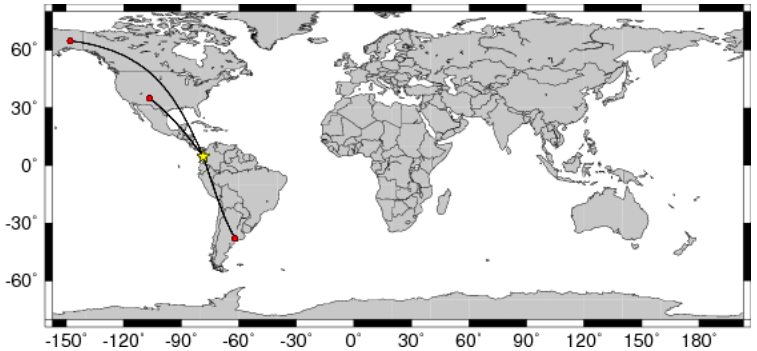

b)

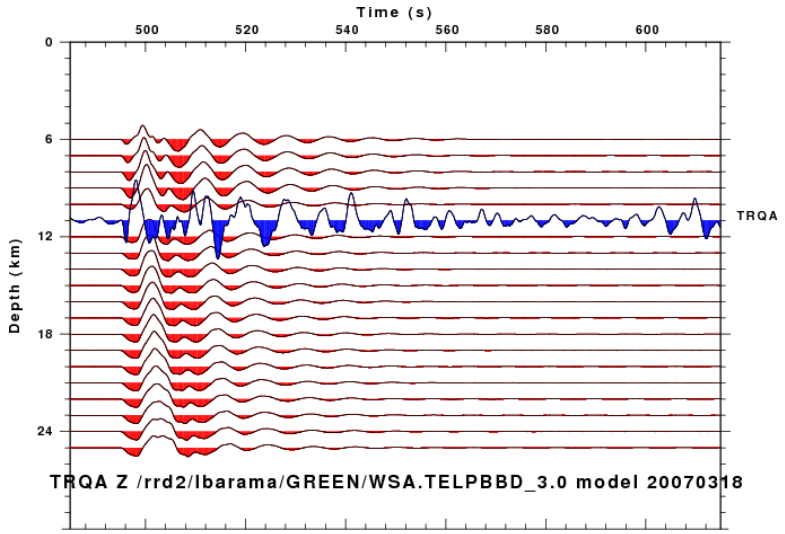

c)

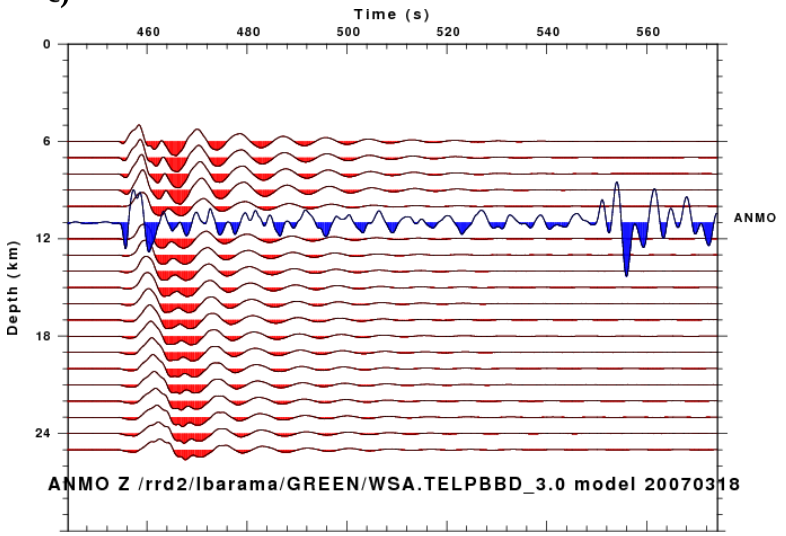

Figure A.11.2 Depth Estimation plots. Refer to description of Figure 4.4.

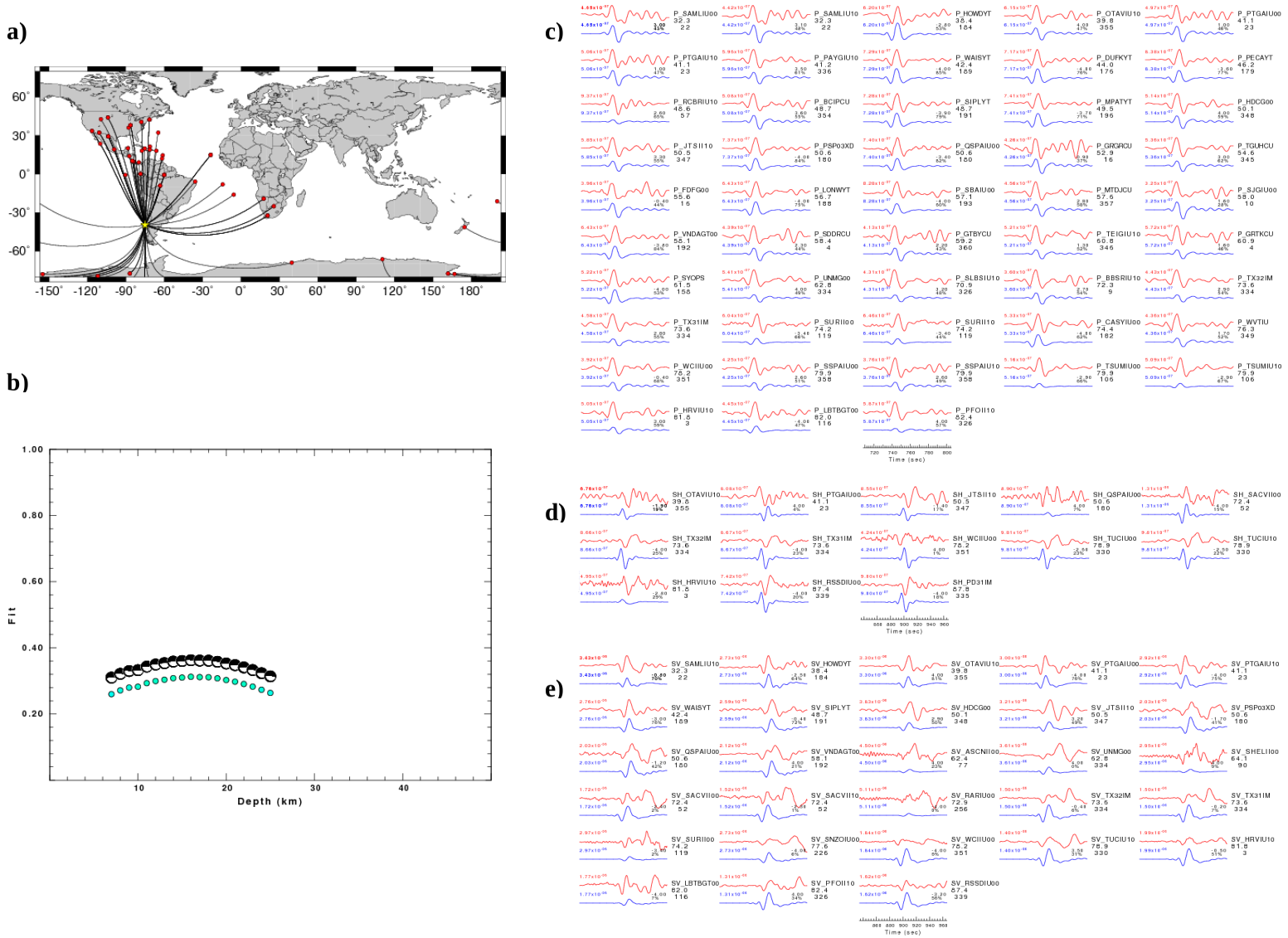

Figure A.12.1 Waveform inversion results for the 11/22/2009 earthquake. Refer to description of Figure 4.3.

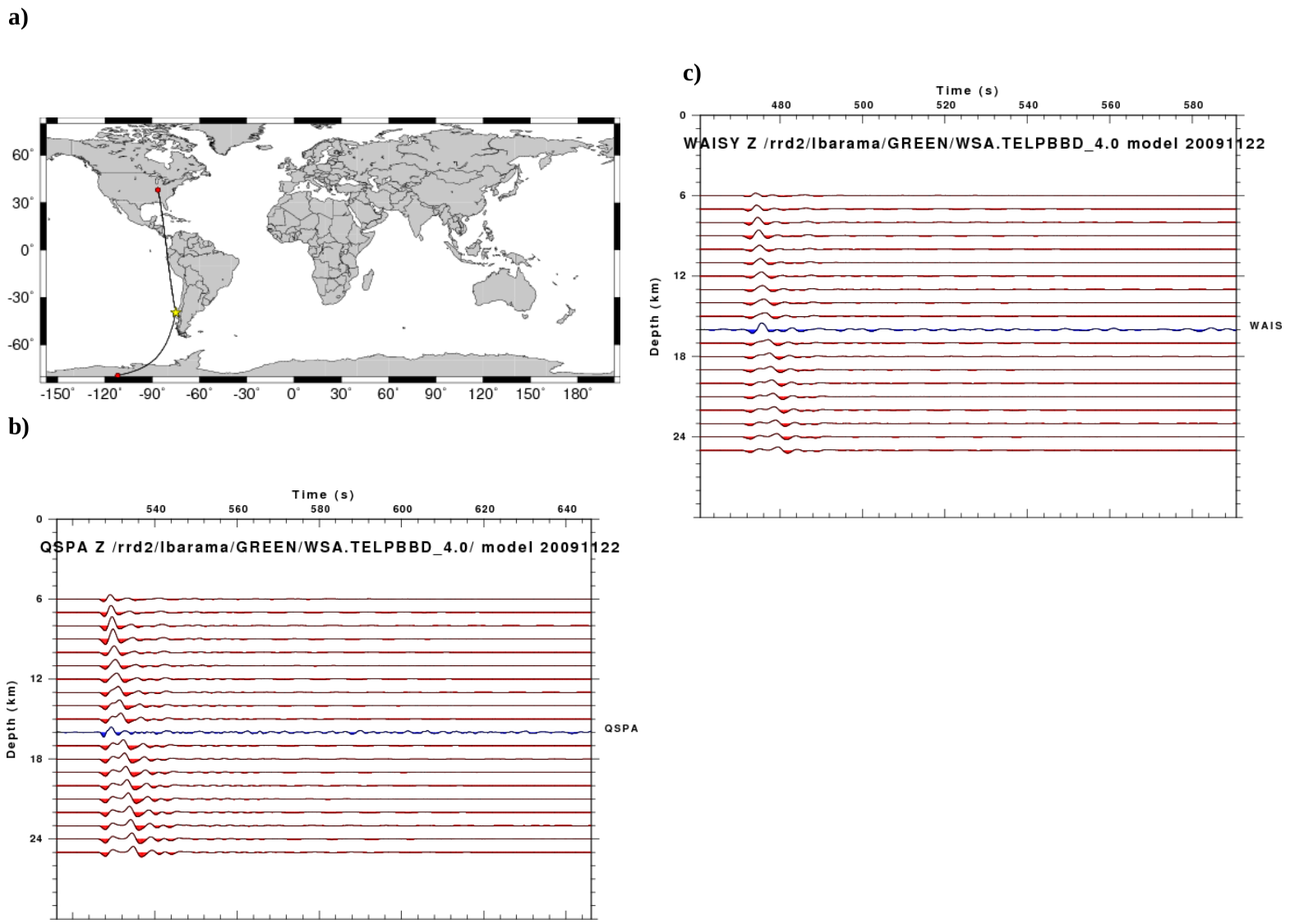

Figure A.12.2 Depth Estimation plots. Refer to description of Figure 4.4.

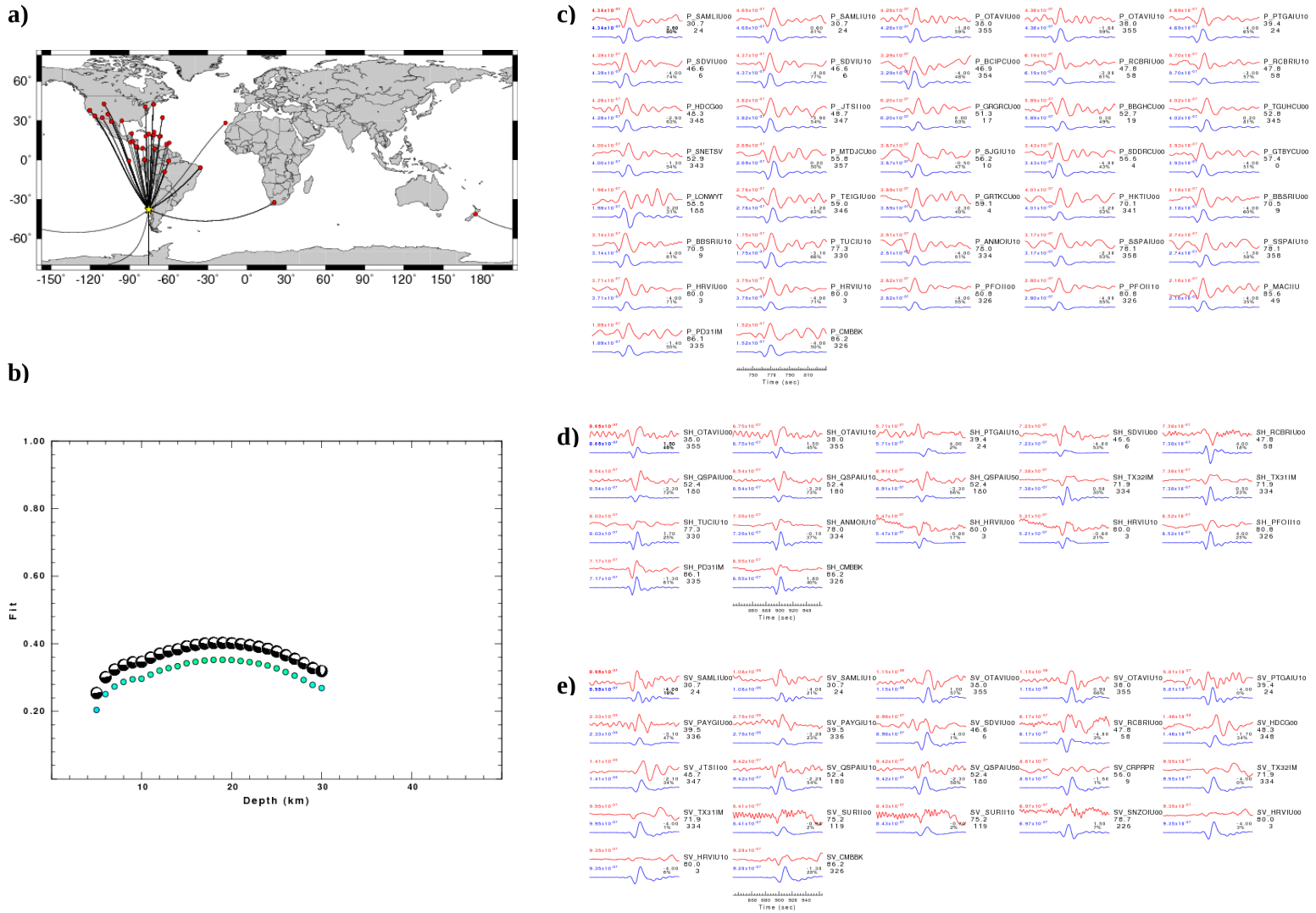

Figure A.13.1 Waveform inversion results for the 06/28/2010 earthquake. Refer to description of Figure 4.3.

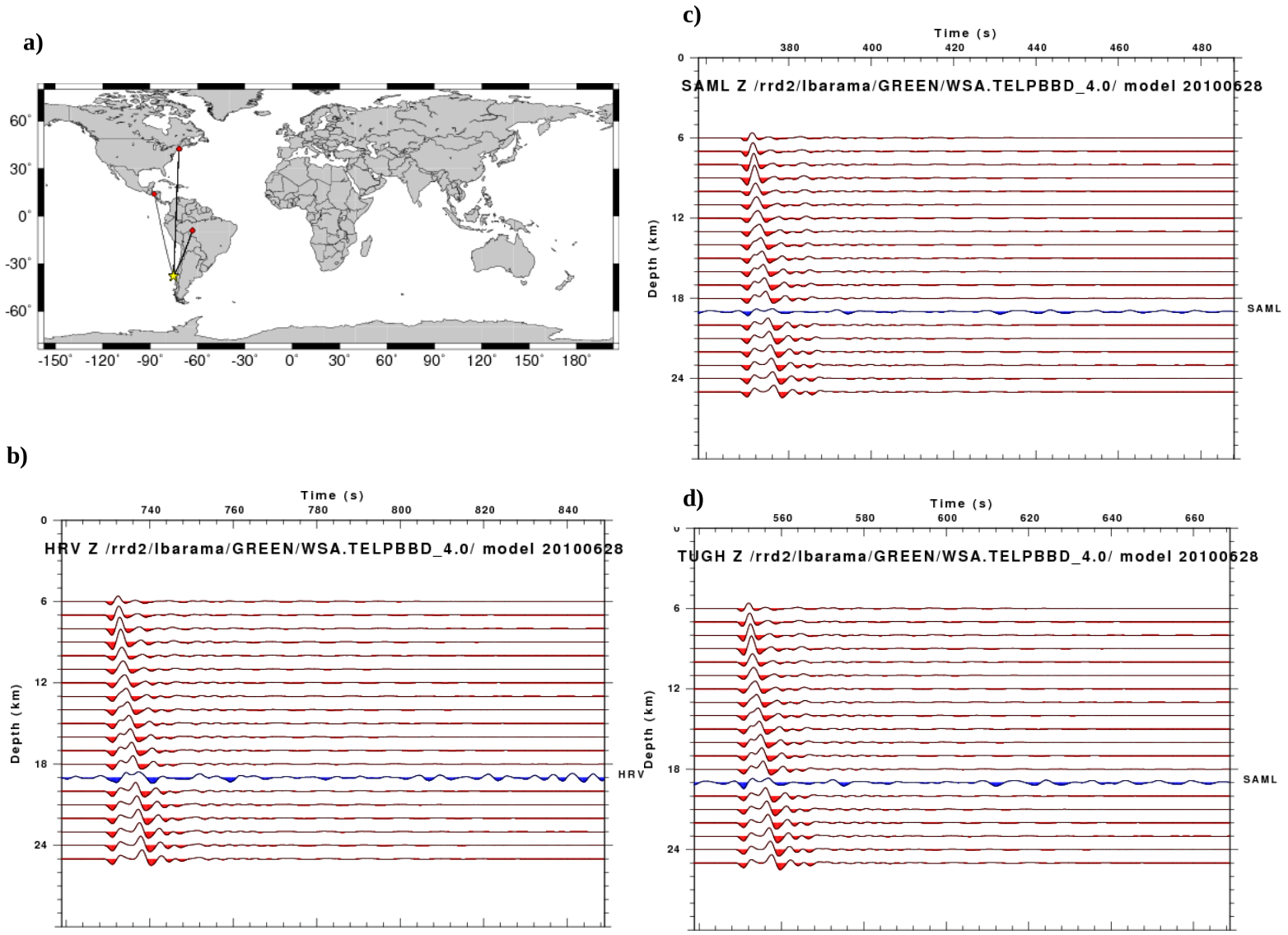

Figure A.13.2 Depth Estimation plots. Refer to description of Figure 4.4.

BIBLIOGRAPHY

Barcheck C.G., D.A. Wiens, P.E. van Keken, and B.R. Hacker (2012), The relationship of intermediate-and deep-focus seismicity to the hydration and dehydration of subducting slabs, *Earth Planet. Sci. Lett.*, 153-160.

Brace, W.F., and D.L. Kohlstedt (1980), Limits on lithospheric stress imposed by laboratory experiments, *J. Geophys. Res.*, 85, 6248-6252.

Caldwell, J.G., W.F. Haxby, D.E. Karig, and D.L. Turcotte (1976), On the applicability of a universal elastic trench profile, *Earth Planet. Sci. Lett.*, 31, 239-246.

Chapple, W.M., and D.W. Forsyth (1979), Earthquakes and bending of plates at trenches, *J. Geophys. Res.*, 84(B12), 6729-6749.

Christensen, D.H., and L.J. Ruff (1988), Seismic coupling and outer rise earthquakes, *Geophys. Res.*,93(B11),13,421-31,444, doi: 10.1029/JB093iB11p13421.

Clouard, V., J. Campos, A. Lemoine, A. Pérez, and E. Kausel (2007), Outer rise stress changes related to the subduction of the Juan Fernández Ridge, central Chile. *J. Geophys. Res.*, 112, doi:10.1029/2005JB003999.

Contreras-Reyes, E., I. Grevemeyer, E.R. Fluej, and M. Scherwath (2007), Alteration of the subducting oceanic lithospere at the southern central Chile trench-outer rise, *Geochem. Geophys. Geosyst*., 8(7), Q07003, doi:10.1029/2007GC001632.

Craig, T.J., A. Copley and J. Jackson (2014), A reassessment of outer-rise seismicity and its implications for the mechanics of oceanic lithosphere, *Geophys. J. Int.* 197**,** 63–89.

Ekström, G., M. Nettles, and A. M. Dziewonski (2012), The global CMT project 2004-2010: Centroid-moment tensors for 13,017 earthquakes, *Phys. Earth Planet. Int.*, 200-201, 1-9, doi:10.1016/j.pepi.2012.04.002.

Emry, E.L., D.A. Wiens, H. Shiobara, and H. Sugioka (2011), Seismogenic characteristics of the Northern Mariana shallow thrust zone from local array data, *Geochem. Geophys. Geosyst.*, 12(12), Q12008, doi: 10.10292011GC003853.

Emry, E.L., D.A. Wiens, and D. Garcia-Castellanos (2014), Faulting within the Pacific plate at the Mariana Trench: Implications for plate interface coupling and subduction of hydrous minerals, *J. Geophys. Res. Solid Earth, 119,* doi:10.1002/2013JB010718.

Fromm, R., P. Alvarado, S. L. Beck, and G. Zandt (2006), The April 9, 2001 Juan Fernández Ridge (M_w 6.7) Tensional Outer-Rise Earthquake and its Aftershock Sequence, *J. Seis.*, 10(2), 163-170.

Garcia-Castellanos, D., M. Torne, and M. Fernàndez (2000), Slab pull effects from a flexural analysis of the Tonga and Kermadec trenches (Pacific Plate*), Geophys. J. Int.*, 141(2), 479–484, doi:10.1046/j.1365-246x.2000.00096.x.

Garcia, P.P., C.A. Vargas, and H. Monsalve (2007), Geometric model of the Nazca plate subduction in Southwest Colombia, *Earth Sci. Res. J.*,11(2), 117-130.

Gill, J. B. (1981), *Orogenic Andesites and Plate Tectonics*, pp. 390, Springer, New York.

Goetze, C., and B. Evans (1979), Stress and temperature in the bending lithosphere as constrained by experimental rock mechanics, Geophys. *J. R. Astron. Soc.*, 59(3), doi:10.1111/j.1365-246X.1979.tb02567.x

Grevemeyer, I., N. Kaul, J.L. Diaz-Naveas, H. Villinger, C.R. Ranero, and C. Reichert (2005), Heat flow and bending-related faulting at subduction trenches: case studies offshore of Nicaragua and Central Chile, *Earth planet. Sci. Lett.*, 236, 238–248.

Grevemeyer, I., C.R. Ranero, , E.R. Flueh, , D. Klaeschen, and J. Bialas (2007), Passive and active seismological study of bending-related faulting and mantle serpentinization at the Middle America trench, *Earth planet. Sci. Lett.*, 258, 528–542.

Gutscher, M.A., W. Spakman, H. Bijwaard and E. R. Engdahl (2000), Geodynamics of flat subduction: Seismicity and tomographic constraints from the Andean margin, *Tectonics*, 19(5), 814-833.

Gutscher, M.A. (2002), Andean subduction styles and their effect on thermal structure and interplate coupling, *J. S. Amer. Earth Sci.*, 15(2002), 3-10, PII:S0895-9811(02)00002-0.

Herrmann, R. B. (1976), Focal depth determination from the signal character of long-period P-waves, *Bull. Seism. Soc. Am.* 66, 1221-1232.

Herrmann, R. B. (2013), Computer programs in seismology: An evolving tool for instruction and research, *Seis. Res. Lett.* 84, 1081-1088, doi:10.1785/0220110096.

Hirschmann, M.M. (2006), Water, melting, and the deep Earth H_2O cycle, *Annu. Rev. Earth Planet. Sci.*, 34, 629–653, doi:10.1146/annurev.earth.34.031405.125211.

Hudson, J.A. (1969), A quantitative evaluation of seismic signals at teleseismic distances, II. Body waves and surface waves from an extended source, *Geophys. J.*,18, 353-370.

Jordan, T.H., and K.A. Sverdrup (1981), Teleseismic location techniques and their application to earthquake clusters in the South-Central Pacific, *Bull. Seis. Soc. Am.*, 71(4), 1105-1130.

Kanamori, H (1971), Seismological evidence for lithospheric normal faulting: the Sanriku earthquake of 1933, *Phys. Earth planet. Int.*, 4, 289-300.

Kirby, S. H. (1980), Tectonic stresses in the lithosphere: Constraints provided by the experimental deformation of rocks, *J. Geophys. Res*., 85, 6353-6363.

Korenaga, J. (2007), Thermal cracking and the deep hydration of oceanic lithosphere: A key to the generation of plate tectonics?, *J.Geophys.Res.*,112,B05408, doi:10.1029/2006JB004502.

Lay, T., L. Astiz, H. Kanamori, and D.H. Christensen (1989), Temporal variation of large intraplate earthquakes in coupled subduction zones, *Phys. Earth Planet. Int.*, 54(3-4), 258-312.

Lefeldt, M., I. Grevemeyer, J. Goßler, and J. Bialas (2009), Intraplate seismicity and related mantle hydration at the Nicaraguan trench outer rise, *Geophys. J. Int.*,178(2), 742-752, doi: 10.1111/j.1365-246X.2009.04167.x.

Lefeldt, M., and I. Grevemeyer (2008), Centroid depth and mechanism of trench-outer rise earthquakes, *Geophys. J. Int.*, 172, 240-251, doi: 10.1111/j.1365-246X.2007.03616.x.

Lomax, A., J. Virieux, P. Volant, and C. Berge (2000), Probabilistic earthquake location in 3D and layered models: introduction of a Metropolis–Gibbs method and comparison with linear locations, in *Advances in Seismic Event Location*, pp. 101–134, eds. Thurber, C.H. & Rabinowitz, N., Kluwer, Amsterdam.

Lonsdale, P. (2005), Creation of the Cocos and Nazca plates by fission of the Farallon plate, *Tectonophysics*, 404, 237-264.

McGinnis, S. (2001), On the effects of geometry in discrete element numerical earthquake simulations, *PhD thesis*, University of Colorado.

McKenzie, D., J. Jackson and K. Priestley (2005), Thermal structure of oceanic and continental lithosphere, *Earth planet. Sci. Lett.*, 233, 337–349.

Moscoso, E., and E. Contreras-Reyes (2012), Outer rise seismicity related to the Maule, Chile 2010 megathrust earthquake and hydration of the incoming oceanic lithosphere, *Geology*, 39(3), 564-572, doi:10.5027/andgeoV39n3-a12.

O'Neill, C., A. M. Jellinek, and A. Lenardic (2007), Conditions for the onset of plate tectonics on terrestrial planets and moons, *Earth Planet. Sci. Lett.*, 261, 20–32, doi:10.1016/j.epsl.2007.05.038.

Peacock, S.M. (2001), Are the lower planes of double seismic zones caused by serpentine dehydration in subducting oceanic mantle, *Geology*, 29(4), 299-302, doi: 10.1130/0091-7613(2001)029<0299:ATLPOD>2.0.CO;2.

Ranero, C. R., J. Phipps Morgan, K. McIntosh, and C. Reichert (2003), Bending related faulting and mantle Serpentinization at the Middle America trench, *Nature*, 425 (6956), 367-373, doi: 10.1038/nature01961.

Ranero, C. R., and V. Sallares (2004), Geophysical evidence for hydration of the crust and mantle of the Nazca plate during bending at the north Chile trench, *Geology*, 32(7), 549-552, doi: 10.1130/G20379.1.

Rüpke, L. H., J. Phipps Morgan, M. Hort, and J.A.D. Connolly (2004), Serpentine and the subduction zone water cycle, *Earth Planet. Sci. Lett.*, 223(1–2), 17–34, doi:10.1016/j.epsl.2004.04.018.

Seno, T., and Y. Yamanaka (1996), Double seismic zones, compressional deep trench-outer rise events and superplumes in Subduction Top to Bottom (G.E. Bebout, D.W. Scholl, S.H. Kirby, J.P. Platt, editors), *Geophysical Monograph*, 96: 347-355.

Shearer, P.M. (2009), *Introduction to Seismology*, *Second Edition*, Cambridge University Press, Cambridge.

Stein, S., and D.A. Weins (1986), Depth Determination fo shallow teleseismic earthquakes: methods and results, *J. Geophys. Res.*, 24(4), 806-832 doi: 10.1029/RG024i004p00806.

Supak, S., D.R. Bohnenstiehl, and W.R. Buck (2006), Flexing is not stretching: An analogue study of flexure-induced fault populations, *Earth Planet. Sci. Lett.* 246, 125–137.

Van Avendonk, H.J.A., W.S. Holbrook, D. Lizarralde, and P. Denyer (2011), Structure and serpentinization of the subducting Cocos plate offshore Nicaragua and Costa Rica, *Geochem. Geophys. Geosyst.,* 12, Q06009, doi:10.1029/2011GC003592.

Van Keken, P.E., B.R. Hacker, E.M. Syracuse, and G.A. Abers (2011), Subduction Factory: 4. Depth-dependent flux of H_2O from subducting slabs worldwide, *J. Geophys. Res.,* 116, B01401, doi: 10.1029/2010JB007922.

Wada, I., M.D. Behn, and A.M. Shaw (2012), Effects of heterogeneous hydration in the incoming plate, slab rehydration, and mantle wedge hydration on slab-derived H_2O flux in subduction zones, *Earth Planet. Sci. Lett.*, 353, 60-71.

Wolfe, C.J., S.C. Solomon, P.G. Silver, J.C. VanDecar, and R.M. Russo (2002), Inversion of body-wave delay times for mantle structure beneath the Hawaiian islands: results from the PELENET experiment, *Earth Planet. Sci. Lett.*, 198(1–2), 129-145.

VITA AUCTORIS

Louisa Barama was born in 1990 in Denmark. She graduated from Brookwood High School in 2008 and received her Bachelor of Science in Physics from Oglethorpe University in 2012. In the Fall of 2012, Louisa began the pursuit of a Master of Science in Geophysics at Saint Louis University.